Molecular Biology of the Cell
Vol. 16, 5592–5609, December 2005

Defects in Structural Integrity of Ergosterol and the Cdc50p-Drs2p Putative Phospholipid Translocase Cause Accumulation of Endocytic Membranes, onto Which Actin Patches Are Assembled in Yeast

Takuma Kishimoto, Takaharu Yamamoto, and Kazuma Tanaka

Division of Molecular Interaction, Institute for Genetic Medicine, Hokkaido University Graduate School of Medicine, N15 W7, Kita-ku, Sapporo 060-0815, Japan

Submitted May 23, 2005; Revised August 24, 2005; Accepted September 15, 2005
Monitoring Editor: Howard Riezman

Specific changes in membrane lipid composition are implicated in actin cytoskeletal organization, vesicle formation, and control of cell polarity. Cdc50p, a membrane protein in the endosomal/*trans*-Golgi network compartments, is a noncatalytic subunit of Drs2p, which is implicated in translocation of phospholipids across lipid bilayers. We found that the *cdc50*Δ mutation is synthetically lethal with mutations affecting the late steps of ergosterol synthesis (*erg2* to *erg6*). Defects in cell polarity and actin organization were observed in the *cdc50*Δ *erg3*Δ mutant. In particular, actin patches, which are normally found at cortical sites, were assembled intracellularly along with their assembly factors, including Las17p, Abp1p, and Sla2p. The exocytic SNARE Snc1p, which is recycled by an endocytic route, was also intracellularly accumulated, and inhibition of endocytic internalization suppressed the cytoplasmic accumulation of both Las17p and Snc1p. Simultaneous loss of both phospholipid asymmetry and sterol structural integrity could lead to accumulation of endocytic intermediates capable of initiating assembly of actin patches in the cytoplasm.

INTRODUCTION

Reorganization of the actin cytoskeleton plays a fundamental role in a variety of cellular processes, including endocytosis and polarized exocytosis. Regulation of actin organization is not thoroughly understood, but specific changes in lipid composition or the production and incorporation of specific lipid species within membranes have been implicated. As such, the role of one group of membrane phospholipids, the phosphoinositides, has been investigated extensively (Janmey and Lindberg, 2004), though other types of lipids may be equally important in this process.

The budding yeast *Saccharomyces cerevisiae* provides an excellent model system to study the regulation of cell and cytoskeletal polarity (Drubin and Nelson, 1996). During budding, the emergence of cell surface extensions is preceded by the polarized organization of two actin filament-containing structures, cortical actin patches and actin cables. This polarized actin organization is triggered by the small GTPase Cdc42p through its effectors, which include formin Bni1p, the PAK kinases Cla4p and Ste20p, and the scaffold proteins Bem1p and Gic1/2p (Pruyne and Bretscher, 2000b). Cortical actin patches are small foci of actin filaments and associated proteins, which cluster near regions of growth. These structures are required for endocytic internalization (Pruyne and Bretscher, 2000a; Engqvist-Goldstein and Drubin, 2003). Among the proteins found in cortical patches are cytoskeletal proteins, including the Arp2/3 complex, its activators (e.g., Pan1p, Abp1p and Las17p) as well as endocytic adaptors (Sla1p and Sla2p; Pruyne and Bretscher, 2000a; Engqvist-Goldstein and Drubin, 2003). Actin cables, which are bundles of actin filaments arising from discrete regions of the plasma membrane coincident with growth sites, serve as tracks for the transport of secretory vesicles by a type V myosin Myo2p (Pruyne and Bretscher, 2000a). Actin cables are assembled by the action of formins Bni1p and Bnr1p, which are capable of polymerizing actin directly (Evangelista *et al.*, 2003).

Previously, we showed that Cdc50p, a conserved membrane-spanning protein, is required for polarized growth (Misu *et al.*, 2003). *cdc50*Δ mutant displays cold-sensitive cell cycle arrest with small buds. Arrested *cdc50*Δ cells are large and round, exhibiting depolarization of cortical actin patches and defective formation of actin cables. Consistent with these phenotypes, Bni1p and Gic1p are mislocalized in *cdc50*Δ mutant cells. Cdc50p localizes primarily to the *trans*-Golgi network (TGN) and endosomal compartments, suggesting that Cdc50p contributes to formation of cell polarity through regulation of vesicular trafficking. More recently, we showed that Cdc50p associates with Drs2p, a putative phospholipid-translocating P-type ATPase, as a noncatalytic β subunit, and that it is required for transport of Drs2p to the TGN and endosomes (Saito *et al.*, 2004).

This article was published online ahead of print in *MBC in Press* (http://www.molbiolcell.org/cgi/doi/10.1091/mbc.E05–05–0452) on September 29, 2005.

Address correspondence to: Kazuma Tanaka (k-tanaka@igm.hokudai.ac.jp).

Abbreviations used: 3HA, three tandem repeats of the influenza virus hemagglutinin epitope; 5-FOA, 5-fluoroorotic acid; DIC, differential interference contrast; EGFP, enhanced green fluorescent protein; GC-MS, gas chromatography-mass spectrometry; GFP, green fluorescent protein; LAT-A, latrunculin-A; mRFP1, monomeric red fluorescent protein 1; PS, phosphatidylserine; TGN, *trans*-Golgi network; TRITC, tetramethylrhodamine B isothiocyanate.

Most cell types display an asymmetric distribution of phospholipids across the plasma membrane. In general, the aminophospholipids phosphatidylserine (PS) and phosphatidylethanolamine are enriched in the inner leaflet facing the cytoplasm, whereas phosphatidylcholine, sphingomyelin, and glycolipids are predominantly found in the outer leaflet. Lipid asymmetry is generated and maintained by ATP-driven lipid transporters or translocases. A subfamily of the P-type ATPases is implicated in translocation of aminophospholipids from the external to the cytosolic leaflet (Pomorski *et al.*, 2004). Drs2p, one of five members of this subfamily in budding yeast, is localized to the endosomal/TGN compartments (Hua *et al.*, 2002; Saito *et al.*, 2004). Drs2p on isolated Golgi membranes can transport a fluorescently labeled analog of PS in an ATP-dependent manner (Natarajan *et al.*, 2004), suggesting that Drs2p is at least in part responsible for generation of phospholipid asymmetry in these membranes. It was suggested that Cdc50p also regulates the phospholipid asymmetry through the interaction with Drs2p (Saito *et al.*, 2004). The *drs2*Δ mutant exhibits TGN defects comparable with those exhibited by strains with clathrin mutations (Chen *et al.*, 1999), supporting the idea that the Cdc50p-Drs2p complex regulates polarized organization of the actin cytoskeleton by modulating vesicle trafficking.

In addition to the phospholipids, the other major membrane components commonly found to be partitioned to the plasma membrane are the sterols (Prinz, 2002). These molecules, which are essential components of eukaryotic membranes, are enriched in the shmoo tips of pheromone-induced budding yeast cells (Bagnat and Simons, 2002) and the leading edge of hyphal growth in *Candida albicans* (Martin and Konopka, 2004). However, it is unknown what, if any, role is played by the sterols in the organization of the actin cytoskeleton. Ergosterol, the major sterol in yeast, is essential for cell viability, but mutants in the last five steps of ergosterol biosynthesis (*erg2* to *erg6*) grow normally. This is the result of accumulation of a distinct set of sterols separate from ergosterol that are able to substitute for the essential activity of ergosterol. The viability of these mutants enables us to analyze whether ergosterol is specifically required for particular cellular processes. For example, combinations of *erg* mutations result in defects in endocytic vesicle transport (Heese-Peck *et al.*, 2002), although no defects in the organization of cortical actin patches were observed.

It is presumed that different lipid species are specifically organized in the membrane bilayer to perform or support a variety of cellular functions. In this study, we searched for genes that functionally interact with *CDC50* by synthetic-lethal screening and have identified *erg3* as an interacting partner. Interestingly, in the *cdc50*Δ *erg3*Δ mutant, actin patches were observed to assemble within the cytoplasmic space in addition to cortical sites. These intracellular actin patches seemed to be assembled on accumulated endocytic membranes. We propose that the lipid environment may be an important determinant of the sites onto which actin patches are assembled.

MATERIALS AND METHODS

Media and Genetic Methods

Strains were cultivated in YPDAW-rich medium (1% yeast extract [Difco Laboratories, Detroit, MI], 2% bacto-peptone [Difco], 2% glucose, 200 μg/ml tryptophan, and 0.01% adenine). Strains carrying plasmids were selected in synthetic medium (SD) containing the required nutritional supplements (Rose *et al.*, 1990). When indicated, 0.5% casamino acids and 200 μg/ml tryptophan were added to SD medium with (SDAW) or without 20 μg/ml uracil (SDAW-Ura). For induction of the *GAL1* promoter, 3% galactose and 0.2% sucrose were used as carbon sources instead of glucose (YPGAW and SGAW-Ura). In synthetic lethal screening, SDA containing 0.1% 5-fluoroorotic acid (5-FOA; Wako Pure Chemicals, Osaka, Japan; SDA + 5-FOA) and YPD-rich medium (1% yeast extract, 2% bacto-peptone, and 2% glucose) were used to counterselect for the presence of *URA3*-containing plasmids, and for the colony sectoring assay, respectively. Standard genetic manipulations of yeast were performed as described previously (Guthrie and Fink, 1991). *Escherichia coli* strains DH5α and XL1-Blue were used for construction and amplification of plasmids. The lithium acetate method was used for introduction of plasmids into yeast cells (Elble, 1992; Gietz and Woods, 2002).

Strains and Plasmids

Yeast strains used in this study are listed in Table 1. Yeast strains carrying complete gene deletions (*lem3*Δ, *cdc50*Δ, *drs2*Δ, and *erg3*Δ), *GAL1* promoter-inducible three tandem repeats of the influenza virus hemagglutinin epitope (3HA)-tagged *CDC50*, enhanced green fluorescent protein (EGFP)-tagged genes (*ABP1*, *PAN1*, *SLA2*, *LAS17*, *MYO5*, *BNI1*, and *GIC1*), and monomeric red fluorescent protein 1 (mRFP1)-tagged *ABP1* were constructed by PCR-based procedures as described (Longtine *et al.*, 1998; Goldstein *et al.*, 1999; Saito *et al.*, 2004). The *erg3*, *erg4*, and *erg6* disruption mutants were constructed as follows. Regions containing the disruption marker and the flanking sequences were PCR-amplified using genomic DNA derived from either the *erg3*Δ*::KanMX6*, *erg4*Δ*::KanMX6*, or *erg6*Δ*::KanMX6* strain (a gift from C. Boone, University of Toronto) as a template. The amplified DNA fragment was then introduced into the appropriate strain. All constructs produced by the PCR-based procedure were verified by colony-PCR amplification to confirm the replacement occurred at the expected locus. The *myo3*Δ *myo5-1* mutant was constructed in the BY4743 background as previously described (Toi *et al.*, 2003). The *erg2*Δ, *erg5*Δ, *vps5*Δ, *vps17*Δ, *vps26*Δ, *vps29*Δ, *vps51*Δ, *vps52*Δ, *vps54*Δ, *ypt6*Δ, and *rcy1*Δ deletion mutants (selectable marker; *KanMX6*) were gifts from C. Boone. The *cdc42-1*, *bni1-116-EGFP bnr1*Δ, *arp2-1*, *las17-11*, *sec2-56*, *sec4-2*, and *lcb1-100* mutants were constructed by three-times backcrosses to BY4743 background strains, whereas the *tpm1-2 tpm2*Δ mutant was constructed by three-times backcrosses to YEF473 background strains.

The plasmids used in this study are listed in Table 2. Schemes detailing the construction of plasmids are available on request.

Gas Chromatography Mass Spectrometry

Total sterols were isolated as previously described (Munn *et al.*, 1999). Cholesterol, as an internal control, was added to total isolated sterols, which were then dried under continuous nitrogen gas and stored at -20°C. Before subjection to gas chromatography-mass spectrometry (GC-MS), dried sterols equivalent to the amount isolated from 1×10^9 cells were dissolved in *N*,*O*-bis(trimethylsilyl)acetoamide (Wako Pure Chemicals) and reacted at 60°C for 30 min. GC-MS was performed on a QP-5000 Gas Chromatograph-Mass Spectrometer system (Shimadzu, Kyoto, Japan) with the following temperature program: column temperature, 1 min at 150°C, 40°C/min to 295°C, and 20 min at 295°C; injector temperature, 250°C; detector temperature, 310°C.

Isolation of Detergent-insoluble Membrane Fractions

Isolation of detergent-insoluble membrane fractions was performed as described previously using an OptimaTLX with TLA120.2 rotor (Beckman Instruments, Palo Alto, CA) for ultracentrifugation (Bagnat *et al.*, 2000). Pma1p was detected by Western blotting with an anti-Pma1p antibody (a gift from Ramon Serrano).

Isolation of cdc50Δ Synthetic Lethal Mutants

Mutants that are synthetically lethal with *cdc50*Δ were screened by the colony-sectoring assay (Koshland *et al.*, 1985). Cultures of KKT31 (*MATα cdc50*Δ *ade2*Δ *ade3*Δ) harboring pYSLU1(*ADE3*, *URA3*)-CDC50 were mutagenized with ethyl methanesulfonate at a dose resulting in ~30% viability and then plated on YPD plates at a density of ~200 colonies per plate. After 5 d of growth at 30°C, solid red colonies lacking white sectors were selected for further analyses. From ~22,000 colonies, 444 clones displayed the desired nonsectoring phenotype. Of these 444 clones, 111 clones failed to grow on SDA + 5-FOA plates. The dependence of the nonsectoring and 5-FOA-sensitive phenotypes on the *cdc50*Δ mutation was tested by transformation with either YCplac111-CDC50 or YCplac111. Sixty-three clones were scored as *CDC50*-dependent. One and 6 clones displayed dependency on *LEM3* or *DNF1*, confirmed by introduction of pRS315-LEM3 or YCplac111-DNF1, respectively. The remaining mutants were crossed with KKT32 (*MATa cdc50*Δ *ade2*Δ *ade3*Δ), and the resulting diploids were subjected to tetrad analysis. Five clones showed 2:2 segregation for the sectoring phenotype, indicating that their synthetic lethalities with *cdc50* mutation were caused by a single mutation. For four of these clones, the candidate genes were cloned by complementation of the 5-FOA-sensitive growth phenotype of the corresponding

Table 1. *S. cerevisiae* strains used in this study

Strain[a]	Genotype	Reference or source
ABY944	*MATa lys2-801 ura3-52 his3Δ-200 trp1-1 leu2-3,112 tpm1-2::LEU2 tpm2Δ::HIS3*	Pruyne *et al.* (1998)
ANS2-3A	*MATα sec2-56 ura3-52 leu2-3,112 his3/4*	A gift from A. Nakano
ANS4–8A	*MATα sec4–2 ura3-52 leu2-3,112 his3/4*	A gift from A. Nakano
DDY1960	*MATa lys2-801 ura3-52 his3Δ-200 leu2-3,112 ade2-101 las17-11::LEU2*	A gift from D. Drubin
DDY0546	*MATα lys2-801 ura3-52 his3Δ-200 trp1Δ-63 leu2Δ-1 sla2-Δ1::URA3*	A gift from D. Drubin
DJYD2-16D	*MATα gal2 ura3 his4 trp1 leu2 cdc42-1*	Johnson and Pringle (1990)
RH2607	*MATa his3 his4 leu2 bar1 lcb1-100*	A gift from H. Riezman
YMW211U	*MATa lys2-801 ura3-52 his3Δ-200 trp1-Δ63 leu2-1 ade2-101 arp2-1::URA3*	Madania *et al.* (1999)
Y3656	*MATα lys2Δ0 ura3Δ0 his3Δ1 leu2Δ0 met15Δ0 can1Δ::MFA1pr-HIS3-MFα1pr-LEU2*	A gift from C. Boone
YEF473	*MATa/α lys2-801/lys2-801 ura3-52/ura3-52 his3Δ-200/his3Δ-200 trp1Δ-63/trp1Δ-63 leu2Δ-1/leu2Δ-1*	Longtine *et al.* (1998)
BY4743	*MATa/α LYS2/lys2Δ0 ura3Δ0/ura3Δ0 his3Δ1/his3Δ1 leu2Δ0/leu2Δ0 met15Δ0/MET15*	Brachmann CB *et al.* (1998)
KKT2	*MATa lys2Δ0 ura3Δ0 his3Δ1 leu2Δ0 met15Δ0*	This study
KKT7	*MATα HphMX4::P_{GAL1}-3HA-CDC50 can1Δ::MFA1pr-HIS3-MFα1pr-LEU2*	This study
KKT9	*MATα cdc50Δ::HphMX4*	This study
KKT12	*MATa erg3Δ::KanMX6*	This study
KKT16	*MATa HphMX4::P_{GAL1}-3HA-CDC50 erg3Δ::KanMX6*	This study
KKT31	*MATα cdc50Δ::HphMX4 ade2Δ::HphMX4 ade3Δ::KanMX6*	This study
KKT32	*MATa cdc50Δ::HphMX4 ade2Δ::HphMX4 ade3Δ::KanMX6*	This study
KKT40	*MATa drs2Δ::KanMX6*	This study
KKT66	*MATα BNI1-EGFP::HIS3MX6*	This study
KKT67	*MATα HphMX4::P_{GAL1}-3HA-CDC50 BNI1-EGFP::HIS3MX6*	This study
KKT68	*MATa erg3Δ::KanMX6 BNI1-EGFP::HIS3MX6*	This study
KKT69	*MATa HphMX4::P_{GAL1}-3HA-CDC50 erg3Δ::KanMX6 BNI1-EGFP::HIS3MX6*	This study
KKT90	*MATa HphMX4::P_{GAL1}-3HA-CDC50 erg3Δ::KanMX6 MYO5-EGFP::HIS3MX6*	This study
KKT108	*MATa LAS17-EGFP::HIS3MX6*	This study
KKT109	*MATa HphMX4::P_{GAL1}-3HA-CDC50 LAS17-EGFP::HIS3MX6*	This study
KKT110	*MATα erg3Δ::KanMX6 LAS17-EGFP::HIS3MX6*	This study
KKT111	*MATα HphMX4::P_{GAL1}-3HA-CDC50 erg3Δ::KanMX6 LAS17-EGFP::HIS3MX6*	This study
KKT121	*MATa GIC1-EGFP::HIS3MX6*	This study
KKT122	*MATa HphMX4::P_{GAL1}-3HA-CDC50 GIC1-EGFP::HIS3MX6*	This study
KKT123	*MATα erg3Δ::KanMX6 GIC1-EGFP::HIS3MX6*	This study
KKT124	*MATa HphMX4::P_{GAL1}-3HA-CDC50 erg3Δ::KanMX6 GIC1-EGFP::HIS3MX6*	This study
KKT141	*MATα lem3Δ::HphMX4*	This study
KKT158	*MATα HphMX4::P_{GAL1}-3HA-CDC50 erg3Δ::KanMX6 ABP1-EGFP::HIS3MX6*	This study
KKT163	*MATα HphMX4::P_{GAL1}-3HA-CDC50 erg3Δ::KanMX6 PAN1-EGFP::HIS3MX6*	This study
KKT190	*MATα drs2Δ::HIS3MX6*	This study
KKT202	*MATa HphMX4::P_{GAL1}-3HA-CDC50 erg3Δ::KanMX6 cdc42-1*	This study
KKT206	*MATα HphMX4::P_{GAL1}-3HA-CDC50 erg3Δ::KanMX6 las17-11::LEU2*	This study
KKT210	*MATa HphMX4::P_{GAL1}-3HA-CDC50 erg3Δ::KanMX6 arp2-1::URA3*	This study
KKT219	*MATα HphMX4::P_{GAL1}-3HA-CDC50 erg3Δ::KanMX6 SLA2-EGFP::HIS3MX6*	This study
KKT223	*MATa CaURA3::P_{GAL1}-3HA-CDC50 erg3Δ::KlLEU2 bni1-116-EGFP::KanMX6 bnr1Δ::HphMX4*	This study
KKT229	*MATa MYO5-EGFP::KanMX6 ABP1-mRFP1::HIS3MX6*	This study
KKT232	*MATa CaURA3::P_{GAL1}-3HA-CDC50 erg3Δ::KlLEU2 MYO5-EGFP::KanMX6 ABP1-mRFP1::HIS3MX6*	This study
KKT234	*MATα LAS17-EGFP::KanMX6 ABP1-mRFP1::HIS3MX6*	This study
KKT237	*MATα CaURA3::P_{GAL1}-3HA-CDC50 erg3Δ::KlLEU2 LAS17-EGFP::KanMX6 ABP1-mRFP1::HIS3MX6*	This study
KKT246	*MATa myo3Δ::HIS3MX6 myo5-1::KanMX6*	This study
KKT247	*MATα cdc50Δ::HphMX4 ade2Δ::HphMX4 ade3Δ::KanMX6 erg3* p[*CDC50, URA3, ADE3*]	This study
KKT248	*MATa lcb1-100*	This study
KKT251	*MATα erg3Δ::KlLEU2*	This study
KKT252	*MATa erg4Δ::KanMX6*	This study
KKT254	*MATa sec2-56*	This study
KKT256	*MATa sec4-2*	This study
YKT477[b]	*MATα lys2-801 ura3-52 his3Δ-200 trp1Δ-63 leu2Δ-1 tpm1-2::LEU2 tpm2Δ::HIS3*	This study
YKT532[b]	*MATα lys2-801 ura3-52 his3Δ-200 trp1Δ-63 leu2Δ-1 bni1-116-EGFP::KanMX6 bnr1Δ::hphMX4*	Kadota *et al.* (2004)

[a] KKT strains are isogenic derivatives of BY4743. For KKT strains, only relevant genotypes are described.

[b] YKT477 and 532 strains are isogenic derivatives of YEF473.

mutant, using a YCp50-LEU2-based genomic library, and subcloning analysis was performed by standard methods.

FM4-64 Labeling

Staining with the lipophilic styryl dye FM4-64 was performed as described previously with minor modifications (Misu *et al.*, 2003). Cells were grown to late logarithmic phase in YPDAW for 12 h at 30°C. Four OD_{600} units of cells were labeled with 32 μM of FM4-64 (Molecular Probes, Eugene, OR) on ice for 30 min. Cells were then washed once with ice-cold YPDAW. Internalization of FM4-64 was initiated by addition of prewarmed YPDAW and the cells were then chased at 30°C for 1 h. Vacuoles were also visualized by growing cells in the presence of FM4-64 as previously described (Seeley *et al.*, 2002).

Microscopic Observations

For observation of EGFP or mRFP1 fusion proteins in living cells, cells were grown in SDA medium at 30°C for the indicated time to an early-log phase, harvested, mounted on microslide glass, and immediately observed. When the effect of latrunculin-A (LAT-A, Wako Pure Chemicals) was examined,

Table 2. Plasmids used in this study

Plasmid	Characteristics	Reference or source
pKT1262 [YCplac111-CDC50]	*CDC50 LEU2 CEN*	Misu *et al*. (2003)
pKT1339 [pRS315-LEM3]	*LEM3 LEU2 CEN*	This study
YCplac111	*LEU2 CEN*	Gietz and Sugino (1988)
YCplac111-DNF1	*DNF1 LEU2 CEN*	This study
pRS416-GFP-SNC1	*GFP-SNC1 URA3 CEN*	Lewis *et al*. (2000)
pRS416-mRFP1-SNC1	*mRFP1-SNC1 URA3 CEN*	This study
pRS316-EGFP-CDC42	*EGFP-CDC42 URA3 CEN*	A gift from Y. Takai
pYSLU1-CDC50	*CDC50 URA3 ADE3 CEN*	This study
pAG60	*CaURA3MX3*	Goldstein *et al*. (1999)
pUG73	*KlLEU2MX3*	Gueldener *et al*. (2002)
pRS315	*LEU2 CEN*	Sikorsiki and Hieter (1989)
pRS315-ERG3	*ERG3 LEU2 CEN*	This study

cells were treated with 100 μM LAT-A by the addition of a 20 mM stock in dimethyl sulfoxide (DMSO) to the medium as described (Ayscough *et al.,* 1997). To observe filamentous actin, cells were cultured to early-midlog phase, fixed in 3.8% formaldehyde, and stained with tetramethylrhodamine B isothiocyanate (TRITC)-phalloidin (Sigma Chemical, St. Louis, MO) as described (Mochida *et al.,* 2002). Sterols and lipid particles were stained with filipin (Sigma; Beh and Rine, 2004) and Nile red (Sigma; Verstrepen *et al.,* 2004), respectively. For quantification of actin patch distribution, cells were scored as having depolarized actin patches if mother cells possessed $\geq$10 patches in small-budded cell population or as having actin patches in the cytoplasmic space if there were $\geq$5 patches that were more than 0.5 μm away from the plasma membrane of the mother cells. Cells were usually observed under Nikon ECRIPS E800 microscope (Nikon Instec, Tokyo, Japan), which was used as described (Saito *et al.,* 2004). Confocal microscopic observation was performed with FV500 laser scanning confocal microscope equipped with Ar and He/Ne lasers and a 100×/1.35 NA plan apo lens (Olympus, Tokyo, Japan), which was operated with Fluoview software (Olympus). For each field, a *z*-series of 0.4-μm slices was scanned and exported as 24-bit TIFF files.

Electron Microscopy

Samples for transmission electron microscopy were prepared as previously described (Kaiser and Schekman, 1990). Thin sections were stained with uranyl acetate and lead citrate, followed by observation at 75 kV using an H-7100 electron microscope (Hitachi, Tokyo, Japan).

RESULTS

Structural Integrity of Ergosterol Is Required for Viability in the Absence of the Cdc50p-Drs2p Complex

The *cdc50*Δ mutant does not grow at 18°C, but grows at a normal rate at 30°C (Misu *et al.,* 2003). To isolate genes involved in the function of *CDC50*, we searched for mutations that display synthetic lethality with *cdc50*Δ mutation at 30°C. By this method, we isolated new alleles of four genes, *erg3* (Figure 1B), *rgp1*, *vps1*, and *srv2*. A complex of Rgp1p and Ric1p stimulates nucleotide exchange of the Ypt6p small GTPase to promote fusion of recycling endocytic vesicles with late Golgi membranes (Siniossoglou *et al.,* 2000). The *cdc50*Δ mutation exhibited synthetic lethality with *ric1*Δ and a temperature-sensitive *ypt6* mutation as well as *rgp1* (our unpublished results), consistent with involvement of

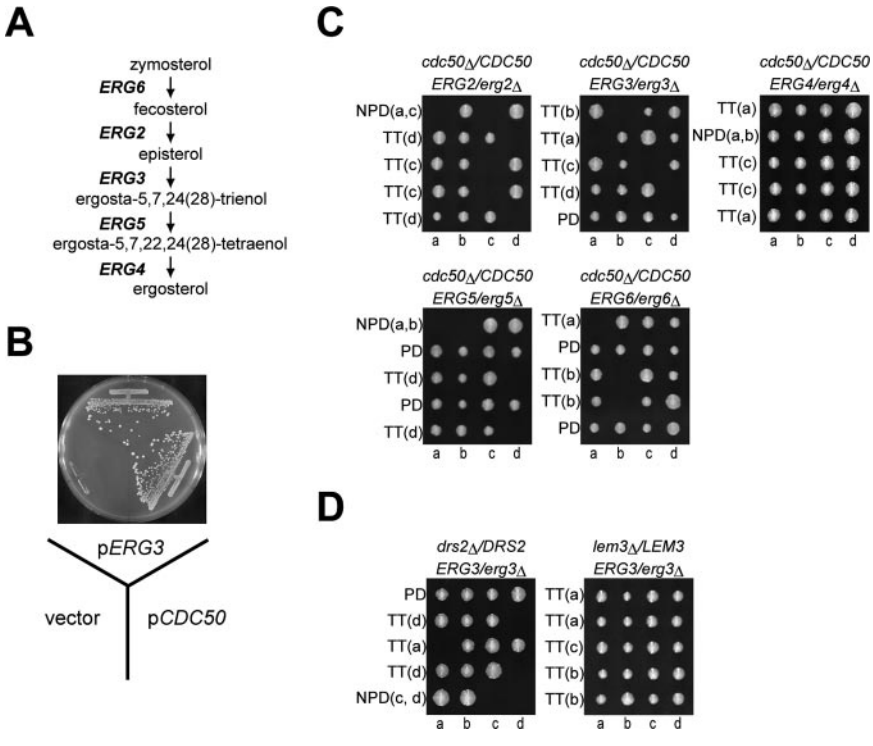

Figure 1. Mutations in *ERG* genes are synthetically lethal with *cdc50*Δ mutation. (A) The late steps of the ergosterol biosynthetic pathway. (B) Synthetic lethality between *cdc50*Δ and *erg3*. *cdc50*Δ *erg3* mutant harboring pYSLU1-CDC50 (KKT247) was transformed with YCplac111 (vector), YCplac111-CDC50 (p*CDC50*), or pRS315-ERG3 (p*ERG3*). Transformants were streaked onto an SDA + 5-FOA plate and grown at 30°C for 2 d. (C) Genetic interactions between the *cdc50*Δ and *erg*Δ mutations. Diploid cells with the indicated genotype were sporulated, dissected, grown at 30°C for 2 d, and photographed. Colonies were replica plated onto selective media to determine the segregation of the marked mutant alleles. Tetrad genotypes (TT, tetratype; PD, parental ditype; and NPD; nonparental ditype) are indicated, and the identities of the double mutant segregants are shown in parentheses. (D) Genetic interactions between the *erg3*Δ and the *drs2*Δ, or *lem3*Δ mutations. Tetrad analysis was performed as in C.

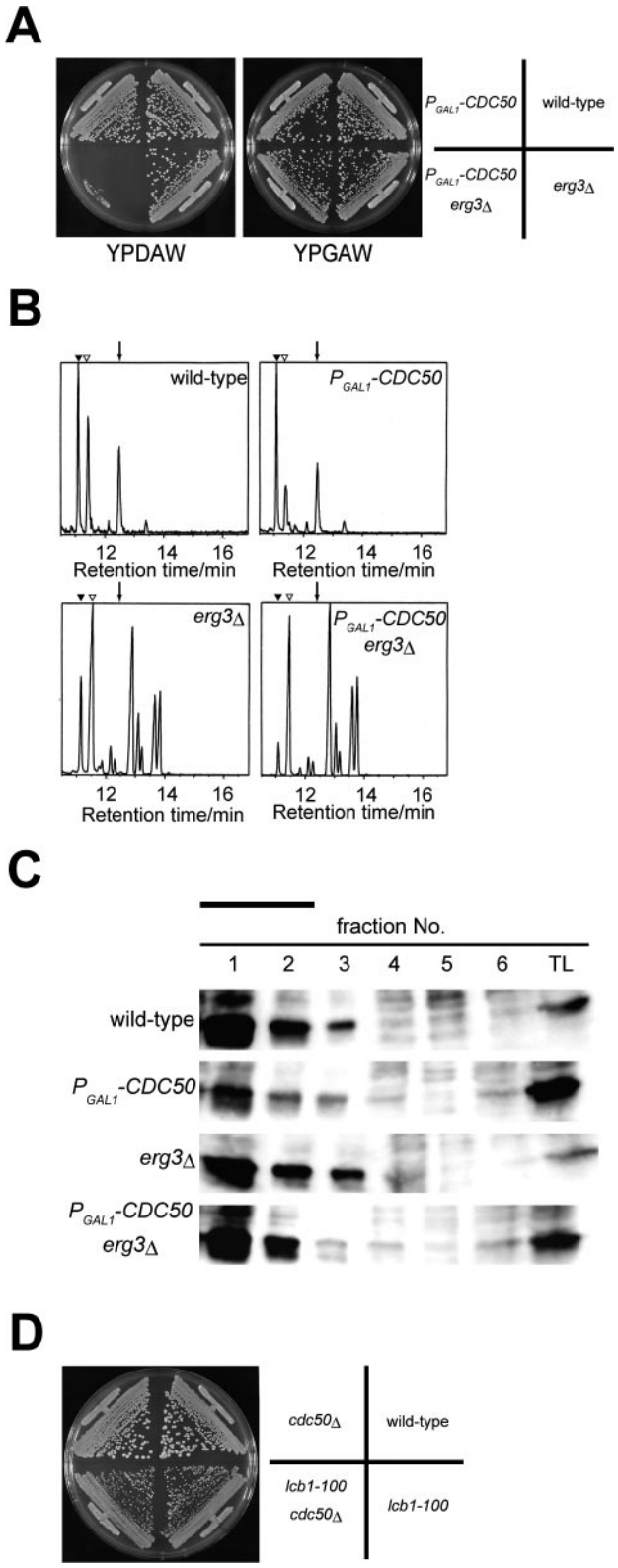

Figure 2. Effect of Cdc50p depletion in the *erg3*Δ mutant on sterol composition and detergent insolubility of Pma1p. (A) Construction of a conditional *cdc50 erg3*Δ mutant. Wild-type (KKT2), P_{GAL1}-*3HA-CDC50* (KKT7), *erg3*Δ (KKT12), and P_{GAL1}-*3HA-CDC50 erg3*Δ (KKT16) strains were streaked onto the plates containing glucose (YPDAW) or galactose (YPGAW) and cultured at 30°C for 2 d. (B) Gas chromatograph of total sterols. Total sterols were isolated from the strains used in A after 9 h of growth in YPDAW at 30°C. Peaks indicated by closed and open triangles represent the background of GC and cholesterol coinjected as a standard, respectively. An arrow indicates the retention time for ergosterol. (C) Association of Pma1p with the detergent insoluble fractions in the P_{GAL1}-*3HA-CDC50 erg3*Δ mutant. Each strain was grown in YPDAW for 9 h at 30°C and detergent-insoluble membrane fractions were isolated. Fractions were collected from the top of the Opti-prep density gradient, followed by the Western blot analysis with the anti-Pma1p antibody (fraction 1, top; fraction 6, bottom in tubes). A solid bar indicates detergent insoluble membrane fractions. TL, total lysate. (D) The *cdc50*Δ mutation does not exacerbate the slow growth phenotype of the *lcb1-100* mutant. Tetra type tetrads from a diploid cell heterozygous for *lcb1-100* and *cdc50*Δ were grown at 30°C. After streaking, YPDAW plates were incubated at 30°C for 2 d. The result shown is a representative of four independent tetrads.

Cdc50p and Drs2p in endocytic recycling (Hua *et al.*, 2002; Saito *et al.*, 2004). Srv2p is also involved in endocytosis as a component of cortical actin patches (Wesp *et al.*, 1997). Vps1p, a dynamin in yeast, has been implicated in clathrin-dependent protein transport at the TGN (Bensen *et al.*, 2000; Gurunathan *et al.*, 2002). Thus, the genetic interaction between *cdc50*Δ and *vps1* is consistent with a suggested role of Drs2p in the formation of clathrin-coated vesicles (Chen *et al.*, 1999).

Erg3p is a sterol C-5 desaturase, which catalyzes a late step in the ergosterol biosynthetic pathway. The observed synthetic lethality with *erg3* thus suggests a functional relationship between phospholipid asymmetry and ergosterol. We decided to investigate the physiological significance of this synthetic lethality. We crossed *cdc50*Δ mutant to mutants deficient in the late steps of the ergosterol biosynthetic pathway (Figure 1A), followed by tetrad analysis. The *cdc50*Δ mutation exhibited synthetic lethality with *erg6*Δ, *erg2*Δ, *erg3*Δ, and *erg5*Δ mutations, but not with the *erg4*Δ mutation, a defect in the terminal step of ergosterol synthesis (Figure 1C). Cdc50p and its homolog, Lem3p, associate with the aminophospholipid translocases Drs2p and Dnf1p, respectively (Saito *et al.*, 2004). The Cdc50p-Drs2p and Lem3p-Dnf1p complexes are functionally redundant, because only simultaneous loss of function of both complexes results in a synthetic growth defect. The *drs2*Δ mutation also exhibited synthetic lethality with *erg3*Δ (Figure 1D), *erg2*Δ, *erg5*Δ, and *erg6*Δ mutations (our unpublished data). However, we did not detect any synthetic growth defect between *lem3*Δ and these *erg*Δ mutations (Figure 1D and our unpublished data). These genetic interactions indicate that the complete ergosterol synthetic pathway is required for cell viability when the Cdc50p-Drs2p putative phospholipid translocase is disrupted.

*Cdc50p Depletion in the erg3*Δ *Mutant Does Not Affect Sterol Composition*

To perform phenotypic analysis of the *cdc50*Δ *erg3* mutant, a conditional mutant of *CDC50* was constructed. We chose to express *CDC50* under the control of the glucose-repressible *GAL1* promoter rather than construct a temperature-sensitive mutant, because the *cdc50*Δ *erg3*Δ double mutant was capable of low-level growth at 37°C (our unpublished data). As shown in Figure 2A, the P_{GAL1}-*3HA-CDC50 erg3*Δ mutant grew normally in galactose-containing medium, but did not grow at all in glucose-containing medium. Because complete growth arrest required incubation for at least 9 h in glucose-containing medium (our unpublished data), phenotypes of the P_{GAL1}-*3HA-CDC50 erg3*Δ mutant (hereafter referred to as

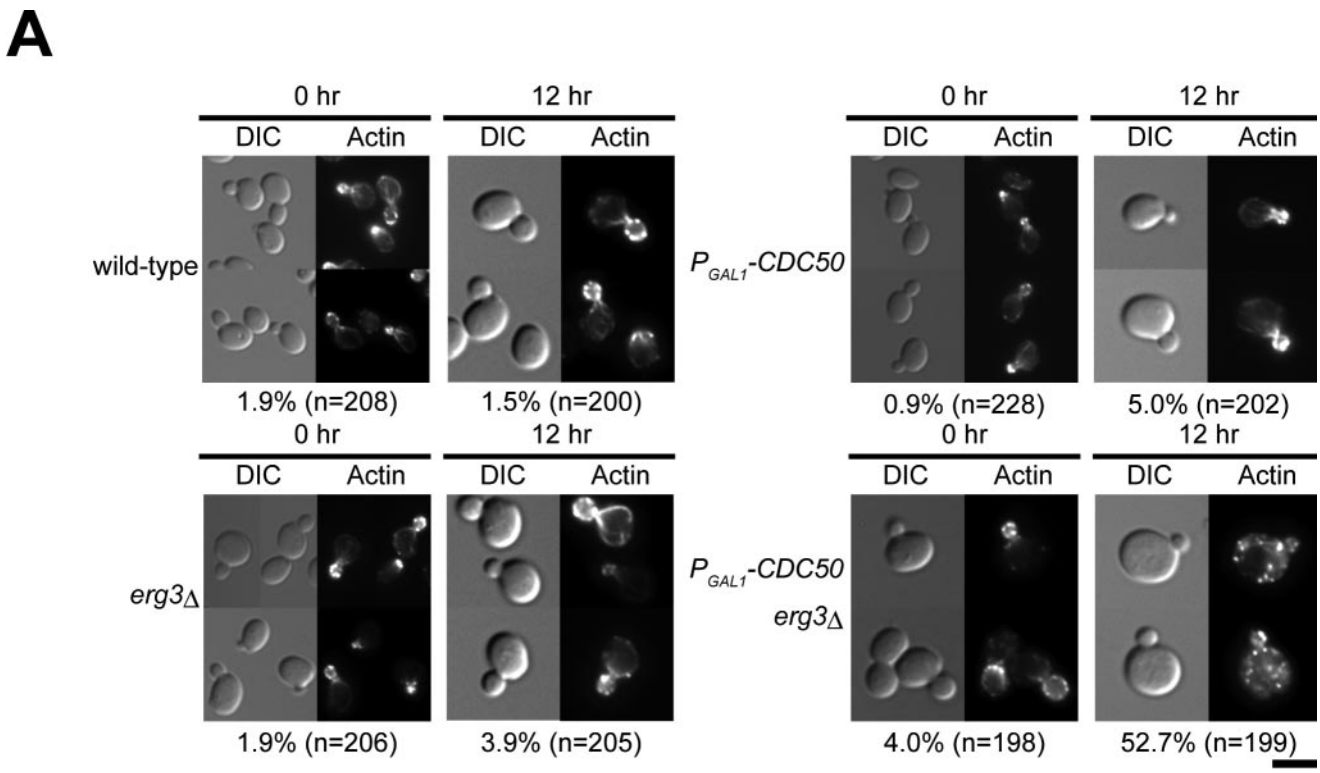

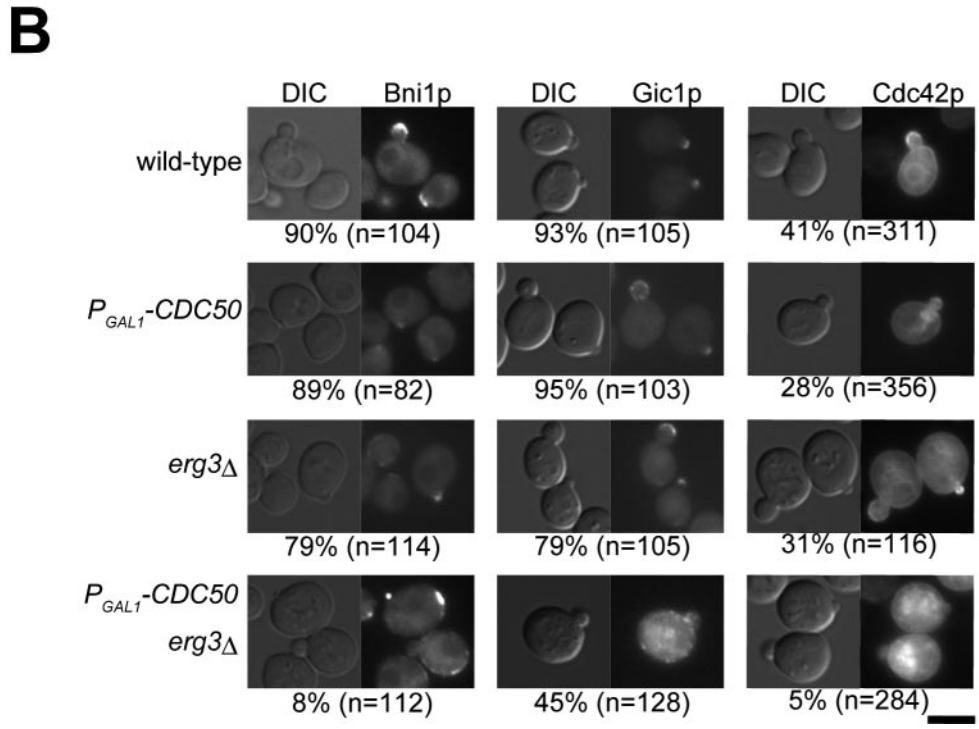

Figure 3. Depletion of Cdc50p causes the depolarization of actin cytoskeleton in *erg3*Δ mutant. (A) F-actin distribution in Cdc50p-depleted *erg3*Δ mutant cells. Strains described in Figure 2A were cultured for the indicated time in YPDAW at 30°C. Cells were fixed, stained with TRITC-phalloidin, and visualized by differential interference contrast (DIC) and epifluorescence. Numbers indicate the percentage of small-budded cells exhibiting the depolarization of actin patches. Bar, 5 μm. (B) Localization of Bni1p-EGFP, Gic1p-EGFP, and EGFP-Cdc42p in Cdc50p-depleted *erg3*Δ mutant cells. Cells were grown in YPDAW medium at 30°C for 12 h. Small-budded cells were scored as having polarized Bni1p-EGFP, Gic1p-EGFP, and EGFP-Cdc42p if they were polarized to bud tip in small-budded cells. Numbers indicate the percentage of small-budded cells exhibiting the normal polarization of these proteins. The strains used were as follows: Bni1p-EGFP-expressing strains; KKT66 (wild-type), KKT67 (P_{GAL1}-*3HA-CDC50*), KKT68 (*erg3*Δ), and KKT69 (P_{GAL1}-*3HA-CDC50 erg3*Δ). Gic1p-EGFP-expressing strains; KKT121 (wild-type), KKT122 (P_{GAL1}-*3HA-CDC50*), KKT123 (*erg3*Δ), and KKT124 (P_{GAL1}-*3HA-CDC50 erg3*Δ). For expression of EGFP-Cdc42p, each strain used in Figure 2A was transformed with pRS316-EGFP-CDC42. Bar, 5 μm.

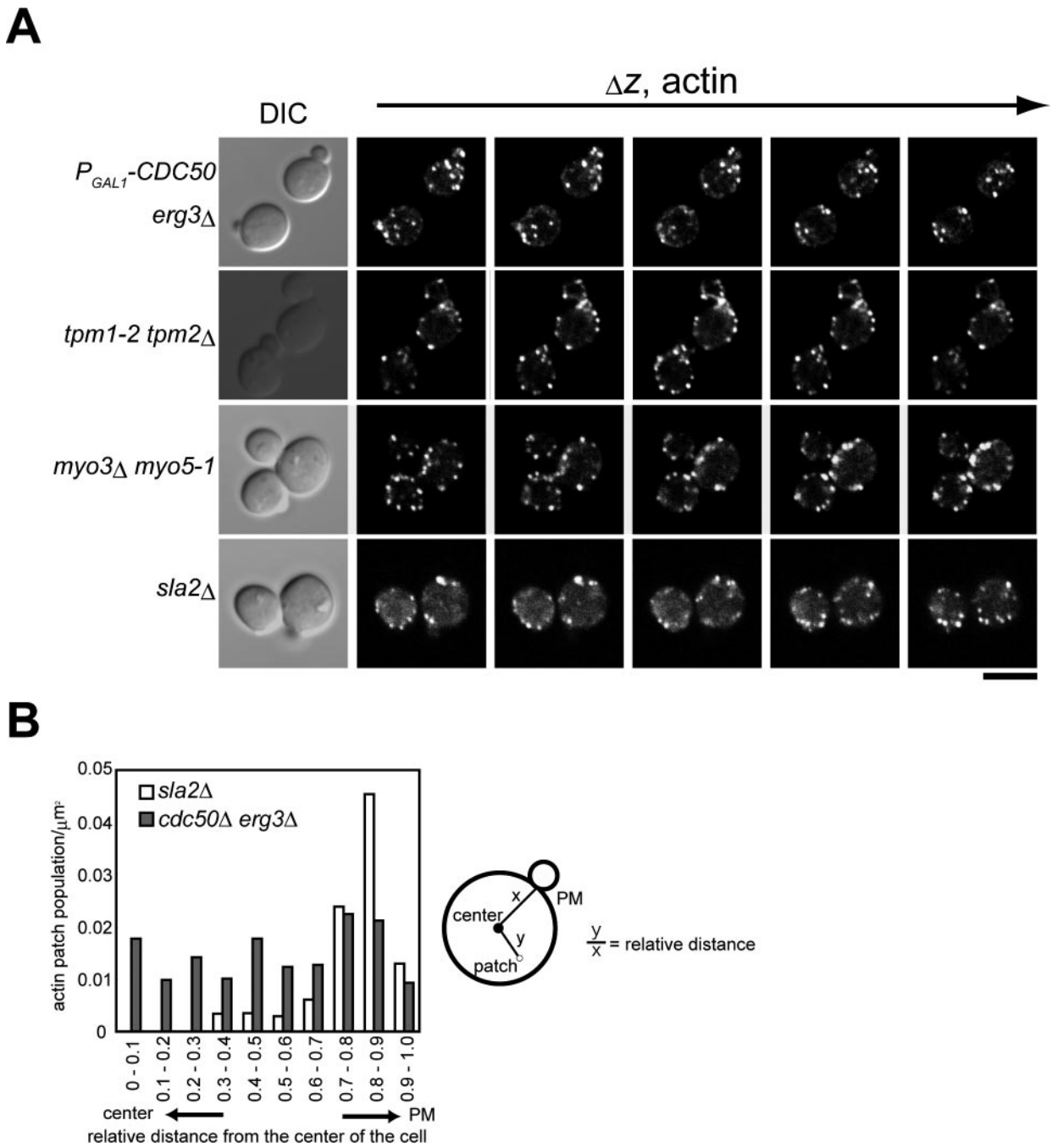

Figure 4. Depletion of Cdc50p results in cytoplasmic assembly of actin patches in the *erg3*Δ mutant. (A) Confocal microscopic observation of actin patch localization. The strain KKT16 (P_{GAL1}-*3HA-CDC50 erg3*Δ) was cultured in YPDAW at 30°C for 12 h. The strains YKT477 (*tpm1-2 tpm2*Δ), KKT246 (*myo3*Δ *myo5-1*), and DDY546 (*sla2*Δ) were cultured in YPDAW at 25°C for 3 h, followed by incubation at 37°C for 2 h. Five consecutive *z*-focal planes (400 nm for each section) traversing a plane with a maximal diameter are shown. Bar, 5 μm. (B) Distribution of cytoplasmic actin patches. The cellular region was divided into 10 subregions in a concentric manner with an even interval from the cell center, and the relative distance from the center of the mother cell was measured for each actin patch in the KKT16 (P_{GAL1}-*3HA-CDC50 erg3*Δ, n = 265 patches from 32 cells) and DDY546 (*sla2*Δ, n = 200 patches from 28 cells) strains, which were cultured as in A. The relative number of actin patches per unit area is presented.

the *cdc50*Δ *erg3*Δ mutant) were analyzed after 9–12 h incubation.

Mutants in late steps of ergosterol synthesis accumulate a variety of sterol derivatives rather than only one ergosterol precursor (Munn *et al.*, 1999; Heese-Peck *et al.*, 2002). When analyzed by GC-MS, the peak pattern and mass spectrum of each peak from the *cdc50*Δ *erg3*Δ mutant were nearly identical to those from the *erg3*Δ mutant. This was also the case when the *cdc50*Δ mutant was compared with the wild-type strain (Figure 2B and our unpublished data). These results suggest that loss of Cdc50p and hence Drs2p does not affect the total sterol composition of the cells. We concluded that

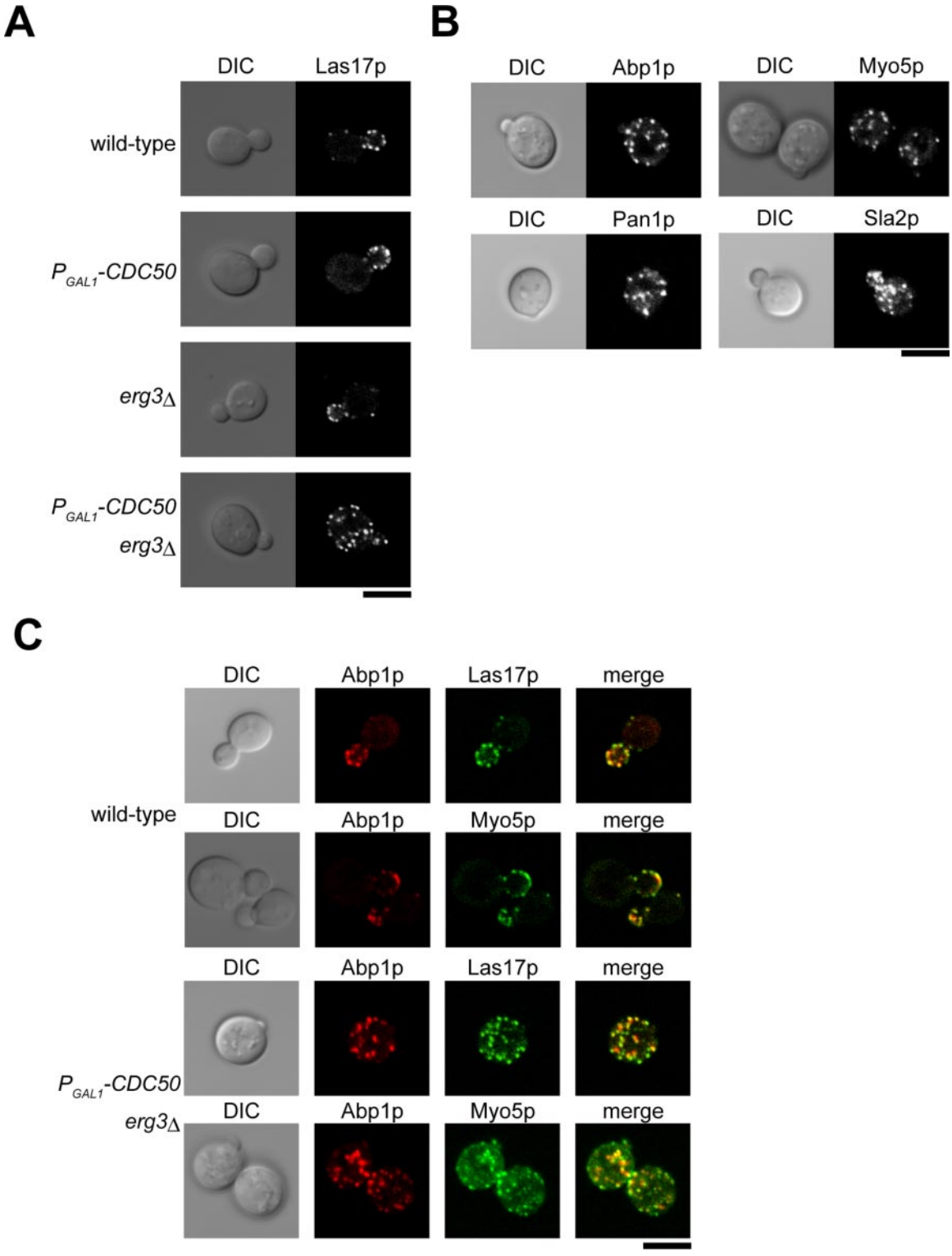

Figure 5. The *cdc50*Δ *erg3*Δ mutant displays cytoplasmic mislocalization of actin patch components. (A) Localization of Las17p-EGFP patches in the *cdc50*Δ *erg3*Δ mutant. The Las17p-EGFP-expressing strains examined were KKT108 (wild-type), KKT109 (P_{GAL1}-*3HA-CDC50*), KKT110 (*erg3*Δ), and KKT111 (P_{GAL1}-*3HA-CDC50 erg3*Δ). Cells were cultured in SDAW at 30°C for 12 h, followed by confocal microscopic observation. Central focal plane images are shown. (B) Localization of other actin patch components in the *cdc50*Δ *erg3*Δ mutant. The strains examined were P_{GAL1}-*3HA-CDC50 erg3*Δ mutant expressing Abp1p-EGFP (KKT158), Myo5p-EGFP (KKT90), Pan1p-EGFP (KKT163), or Sla2p-EGFP (KKT219). Cells were cultured and images were acquired as in A. (C) Colocalization of Abp1p-mRFP1 with Las17p-EGFP and Myo5p-EGFP in the *cdc50*Δ *erg3*Δ mutant. The strains examined were KKT234 (wild-type) and KKT237 (P_{GAL1}-*3HA-CDC50 erg3*Δ) expressing both Las17p-EGFP and Abp1p-mRFP1, and KKT229 (wild-type) and KKT232 (P_{GAL1}-*3HA-CDC50 erg3*Δ) expressing both Myo5p-EGFP and Abp1p-mRFP1. Cells were cultured and images were acquired as in A. Bars, 5 μm.

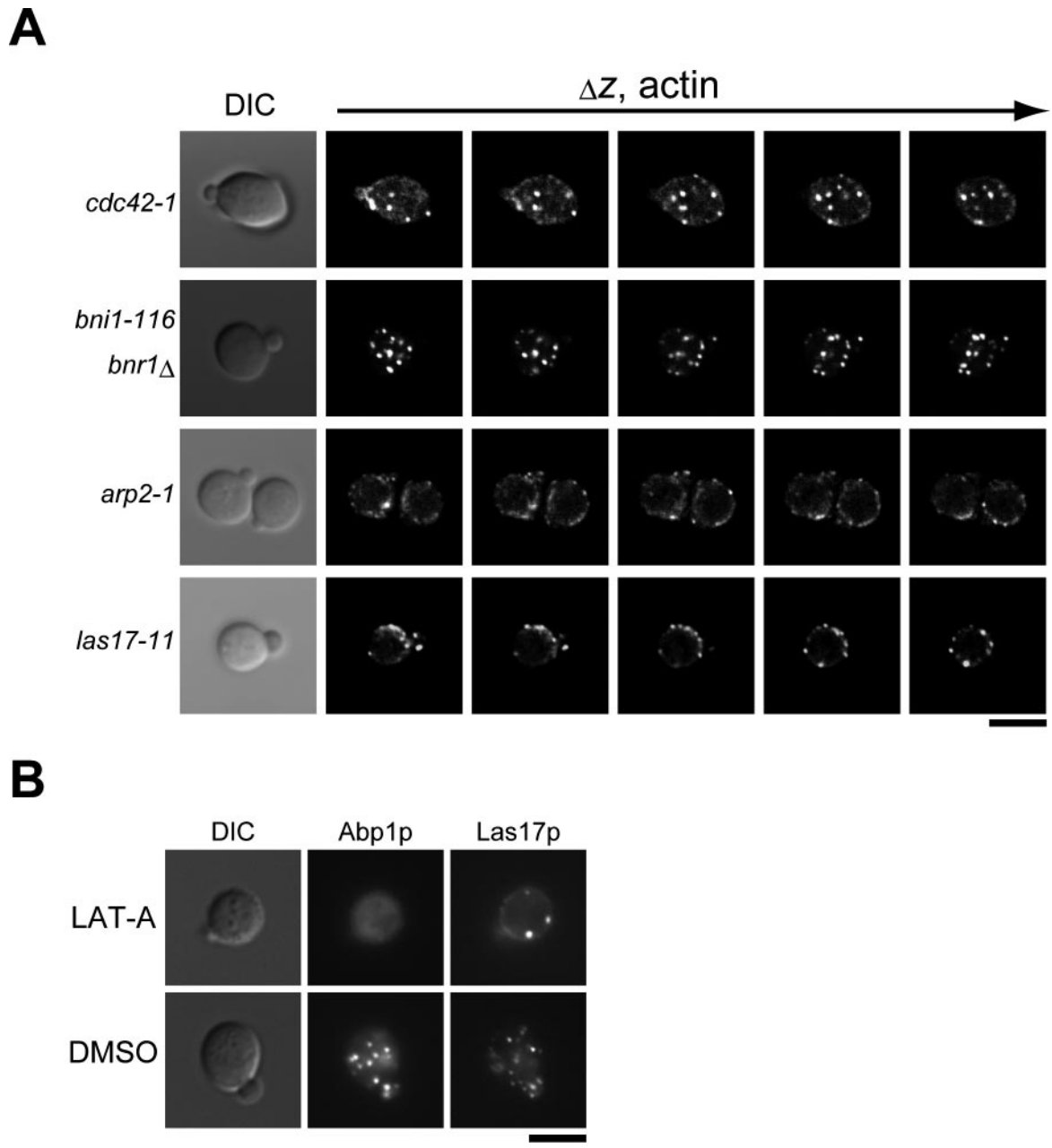

Figure 6. Cytoplasmic assembly of actin patches in the *cdc50*Δ *erg3*Δ mutant is dependent on endocytosis. (A) The effect of mutations in actin-related genes on the localization of actin patches in the *cdc50*Δ *erg3*Δ mutant. *cdc50*Δ *erg3*Δ mutants carrying an additional mutation, *cdc42-1* (KKT202), *bni1-116-EGFP bnr1*Δ (KKT223), *arp2-1* (KKT210), or *las17-11* (KKT206) were cultured in YPDAW at 30°C for 8 h, followed by an additional 2 h culture at 37°C. TRITC-phalloidin staining was performed as described in Figure 3A. Five *z*-focal planes obtained by confocal microscopic observation are shown. Bar, 5 μm. (B) Effects of LAT-A on the localization of actin patch components in the *cdc50*Δ *erg3*Δ mutant. The strain KKT237 (P_{GAL1}-*3HA-CDC50 erg3*Δ) doubly expressing Abp1p-mRFP1 and Las17p-EGFP was cultured in SDAW at 30°C for 8 h, followed by an additional 1-h culture in the presence (LAT-A) or absence (DMSO) of 100 μM LAT-A. Central confocal images are shown. Bar, 5 μm.

the synthetic lethality of the *cdc50*Δ *erg3*Δ mutant is not the result of drastic changes in sterol composition.

Sterol- and sphingolipid-rich detergent-resistant membrane domains (so-called lipid rafts) are implicated in diverse cellular processes including polarized traffic, signal transduction, and endo- and exocytosis (Lucero and Robbins, 2004). In budding yeast, several proteins including the plasma membrane [H^+]ATPase Pma1p have been shown to be associated with detergent insoluble fractions, and their association requires the presence of sterols (Bagnat *et al.*, 2000). Thus, we examined the detergent insolubility of a commonly used marker Pma1p in wild-type, *cdc50*Δ, *erg3*Δ, and *cdc50*Δ *erg3*Δ strains. As shown in Figure 2C, the detergent insolubility of Pma1p was not significantly affected by the *cdc50*Δ, *erg3*Δ, or *cdc50*Δ *erg3*Δ mutation, suggesting that the lethality of the *cdc50*Δ *erg3*Δ mutant may not be attributed to defects in association of Pma1p with the detergent insoluble fractions. We further examined whether *cdc50*Δ

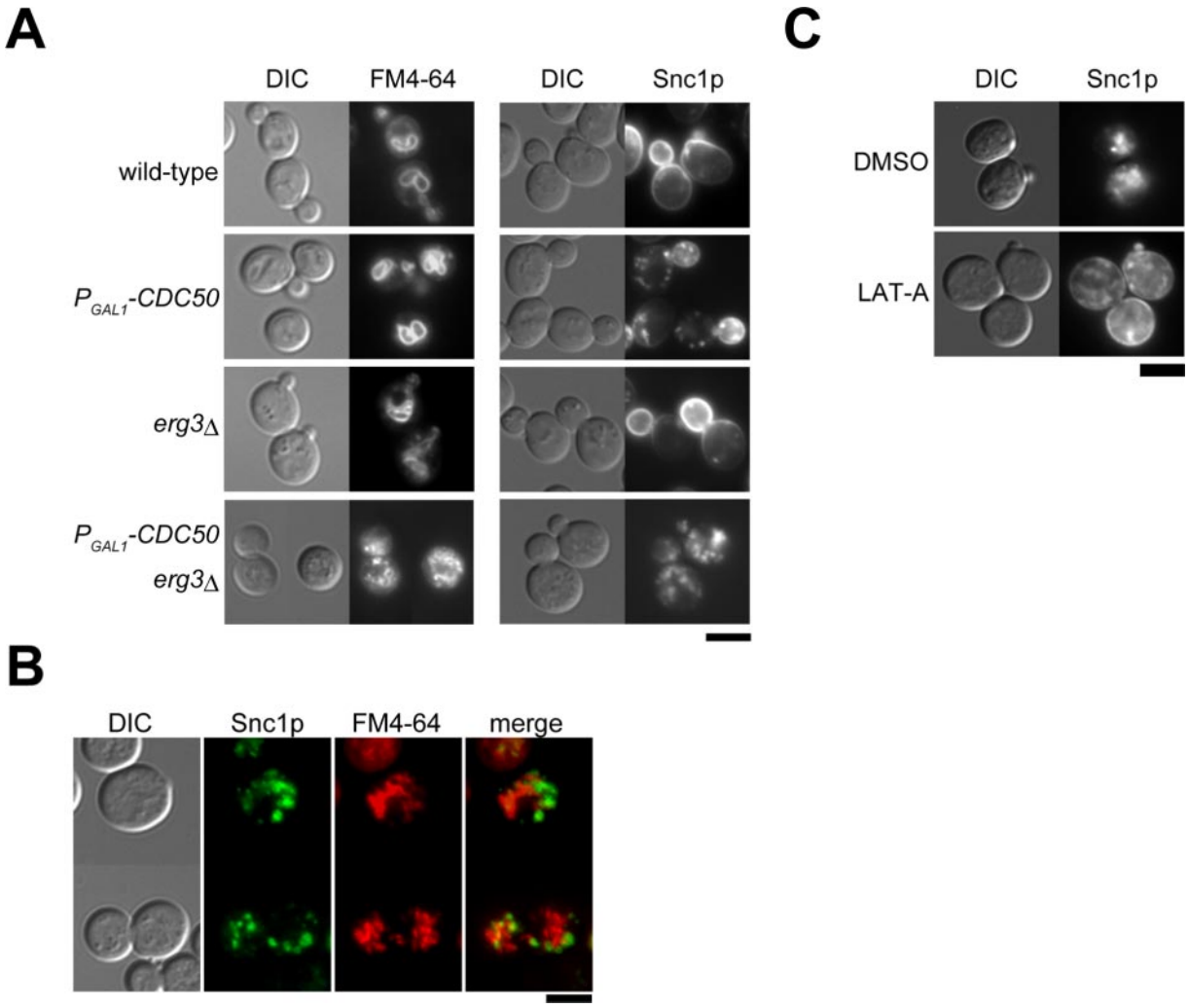

Figure 7. Defective endocytic recycling in the *cdc50*Δ *erg3*Δ mutant. (A) Endocytic internalization and recycling in the *cdc50*Δ *erg3*Δ mutant. Internalization and delivery of FM4-64 to the vacuole was performed as described in *Materials and Methods*. Strains used in Figure 2A were cultured in YPDAW at 30°C for 12 h. To examine localization of GFP-Snc1p, each strain was transformed with pRS416-GFP-SNC1, and cells were cultured in SDAW-Ura at 30°C for 9 h. (B) GFP-Snc1p is not mislocalized to fragmented vacuoles. The strain KKT16 (P_{GAL1}-*3HA-CDC50 erg3*Δ) carrying pRS416-GFP-SNC1 was cultured in SDAW-Ura containing FM4-64 for vacuole staining at 30°C for 12 h. Images are central focal planes. (C) GFP-Snc1p accumulated in the *cdc50*Δ *erg3*Δ mutant is derived from endocytosis. The strain used in B was cultured in SDAW-Ura at 30°C for 8 h, followed by an additional 1-h culture in the presence (LAT-A) or absence (DMSO) of 100 μM LAT-A. Bars, 5 μm.

mutation genetically interacted with a mutation in the essential gene *LCB1*, which encodes serine palmitoyltransferase. Lcb1p, which catalyzes the first step in ceramide and sphingolipids syntheses, is also required for association of Pma1p with detergent-insoluble fractions (Bagnat *et al.*, 2000). However, the *cdc50*Δ mutation did not exacerbate the slow growth phenotype of the *lcb1-100* mutant (Figure 2D).

The cdc50Δ erg3Δ Mutant Intracellularly Assembles Cortical Actin Patches

We examined the morphological phenotype of the *cdc50*Δ *erg3*Δ mutant at 30°C, a temperature at which the *cdc50*Δ single mutant shows normal spherical morphology with polarized organization of the actin cytoskeleton. When *CDC50* expression was repressed, the *cdc50*Δ *erg3*Δ mutant exhibited large and round cell morphology, with the high-frequency appearance of small buds (48%, n = 388; Figure 3A), a phenotype similar to that of *cdc50*Δ cells arrested at

Table 3. Synthetic lethal interactions between *erg3*Δ and mutations that impair membrane traffic

Functions	Mutation
Viable	
Retrograde transport from late endosomes	*vps5*Δ, *vps17*Δ, *vps26*Δ, *vps29*Δ
Endocytic internalization	*las17–11*, *arp2–1*
Late stages of exocytosis	*sec2–56*, *sec4–2*
Inviable	
Endocytic recycling	*vps51*Δ, *vps52*Δ, *vps54*Δ, *ypt6*Δ, *rcy1*Δ

Viability of the double mutant was inferred from the growth phenotype of the tetrad segregants.

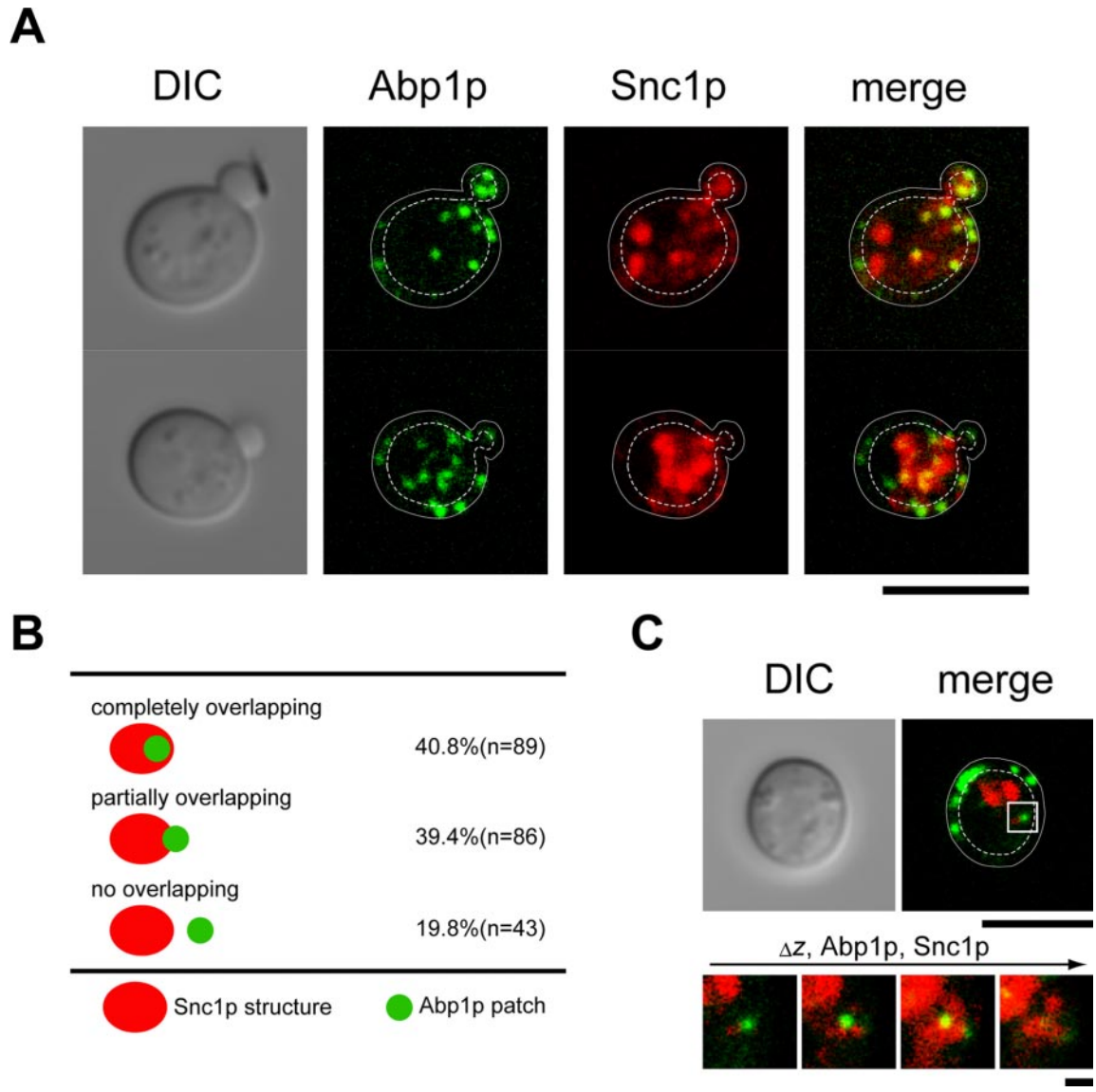

Figure 8. Assembly of actin patches on the internal membranes containing unrecycled Snc1p. (A) Localization of Abp1p-EGFP and mRFP1-Snc1p in the *cdc50*Δ *erg3*Δ mutant. The strain KKT158 (P_{GAL1}-*3HA-CDC50 erg3*Δ *ABP1-EGFP*) harboring pRS416-mRFP1-SNC1 was cultured in SDAW-Ura at 30°C for 12 h, followed by confocal microscopic observation. To distinguish between Abp1p-EGFP patches that appear to function in the normal endocytic pathway and those assembled intracellularly, the cell periphery and a position 500 nm distant from the plasma membrane are indicated with solid and broken lines, respectively (see text). Images are central focal planes. Bar, 5 μm. (B) The proportion of intracellular Abp1p-EGFP patches that showed colocalization with Snc1p structures. Intracellular actin patches (218 patches from 25 cells) were categorized according to their colocalization patterns with mRFP1-Snc1p. (C) Serial sections of an Abp1p-EGFP patch that was not colocalized with the Snc1p structure in one focal plane. Lower images represent four consecutive *z*-focal planes of an Abp1p-EGFP patch that did not show colocalization with mRFP1-Snc1p in a central focal plane (a square of the top merged image and the left most image of bottom images). These images were acquired in 2 s during which significant movement of actin patches was not observed. Representative images of 30 individual actin patches examined are shown. Cortical actin patches are distinguished as in A. Bars in top and bottom images are 5 μm and 100 nm, respectively.

18°C (Misu *et al.*, 2003). In addition, the *cdc50*Δ *erg3*Δ mutant exhibited depolarization of the actin cytoskeleton. In these cells, actin cables were visible in only 6% of the observed cells (n = 158), and cortical patches were found to be evenly distributed throughout the mother cell in 53% (n = 199) of the small-budded cells (Figure 3A). We also examined the localization of the polarity regulator Cdc42p and its effectors, Bni1p and Gic1p, in the *cdc50*Δ *erg3*Δ mutant. Both Bni1p-EGFP and Gic1p-EGFP were mislocalized beneath the plasma membrane in small-budded *cdc50*Δ *erg3*Δ mutant mother cells (Figure 3B). EGFP-Cdc42p was not properly localized to the bud tip and instead accumulated in intracellular membranous structures in small-budded *cdc50*Δ *erg3*Δ cells (Figure 3B). These results suggest that loss of both the Cdc50p-Drs2p putative phospholipid translocase and the integrity of the ergosterol biosynthesis pathway results in depolarized cell growth, probably because of defects in polarized organization of the actin cytoskeleton resulting from mislocalization of Cdc42p and its effectors.

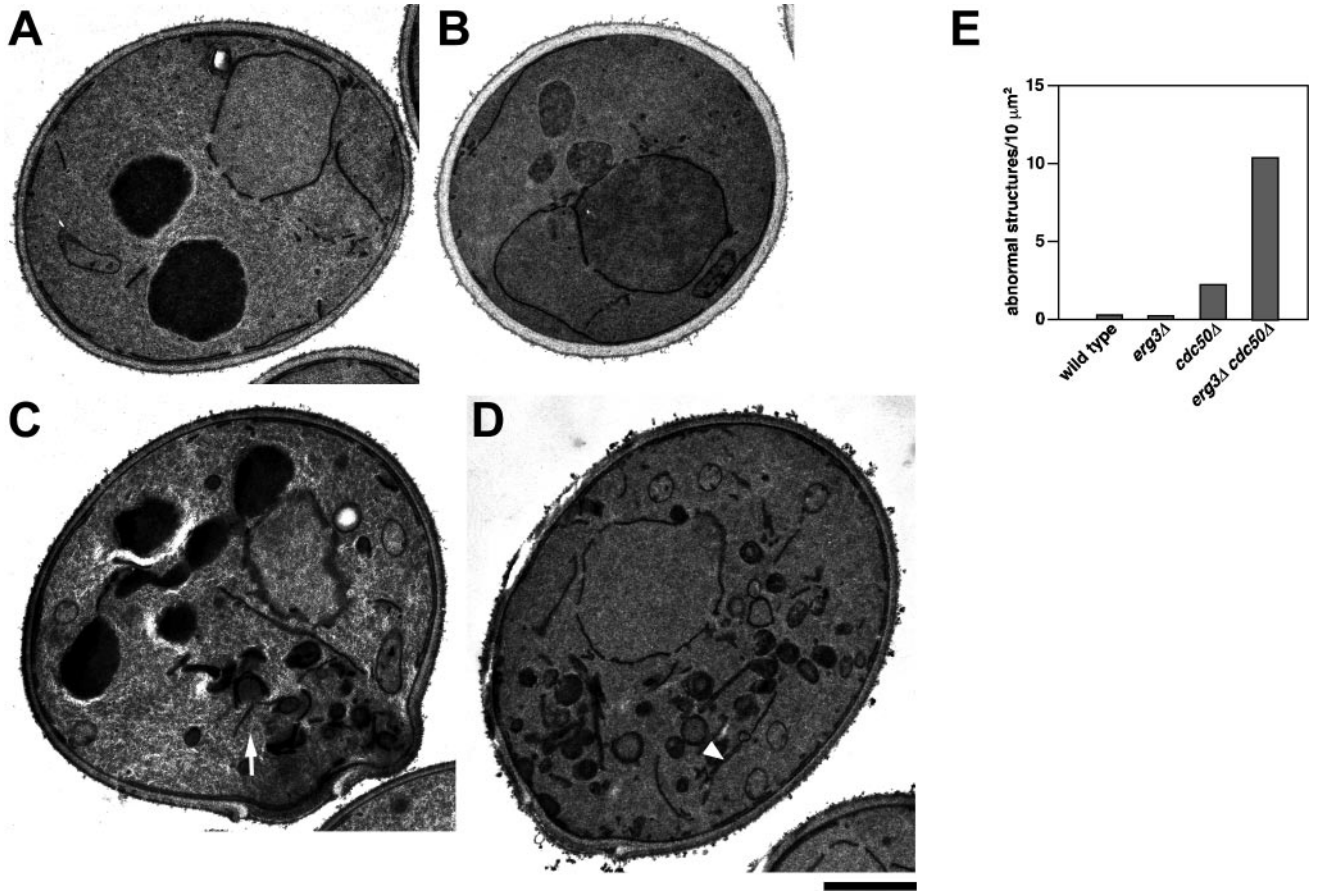

Figure 9. Electron microscopic observation of the *cdc50*Δ *erg3*Δ mutant cell. Wild-type (KKT2, A), *erg3*Δ (KKT12, B), P_{GAL1}-*3HA-CDC50* (KKT7, C), and P_{GAL1}-*3HA-CDC50 erg3*Δ (KKT16, D) cells were cultured in YPDAW at 30°C for 9 h. The cells were fixed with glutaraldehyde and potassium permanganate, followed by an electron microscopic observation. An arrowhead and an arrow indicate representative double-membrane structures with ring and crescent-shaped morphology, respectively. Bar, 1 μm. (E) Quantitation of abnormal and large (>200 nm in diameter) double membranous structures. Bars represent the number of those structures per 10 μm^2. Thirty cell sections were examined for each strain.

In the *cdc50*Δ *erg3*Δ mutant, we observed depolarized filamentous actin patches not only at the cortical region but also in the cytoplasmic space (Figure 4A). After 12 h of growth in glucose medium, 44% of the actin patches in mutant mother cells (n = 265 patches from 32 cells) were present in the cytoplasmic space. These intracellular actin patches were randomly distributed in terms of distance from the plasma membrane (gray bars in Figure 4B). This phenotype was specific to the *cdc50*Δ *erg3*Δ mutant and was not observed in actin-related mutants. Mutants of cortical actin patch assembly, *sla2*Δ (Wesp *et al.*, 1997) and *myo3*Δ *myo5-1* (Geli and Riezman, 1996), and actin cable assembly, *tpm1-2 tpm2*Δ (Pruyne *et al.*, 1998), assembled actin patches only at cortical sites (Figure 4, A and B), although, in the *sla2*Δ mutant, some actin patches were localized at a short distance from the plasma membrane as described (Kaksonen *et al.*, 2003). These results suggest that the actin cytoskeleton of the *cdc50*Δ *erg3*Δ mutant is disorganized in a fundamentally different manner from that of the known actin patch- or actin cable-deficient mutants.

Given the morphological similarity between the cytoplasmic and cortical actin patches, we examined the localization of actin patch assembly proteins in the *cdc50*Δ *erg3*Δ mutant. In wild-type cells, these proteins colocalize with cortical actin patches to a partial (Las17p, Pan1p, Myo5p, and Sla2p) or a full (Abp1p) extent (Engqvist-Goldstein and Drubin, 2003). Both *cdc50*Δ and *erg3*Δ single mutant cells exhibited normal polarized localization for all examined proteins (Figure 5A and our unpublished data). In contrast, 60% of small-budded *cdc50*Δ *erg3*Δ mutant cells displayed apparent mislocalization of Las17p-EGFP patches to the cytoplasmic space (n = 146). Examination of cells expressing Abp1p-EGFP, Myo5p-EGFP, Pan1p-EGFP, and Sla2p-EGFP in the context of *cdc50*Δ *erg3*Δ mutation also revealed similar profiles of cytoplasmic patch staining (Figure 5B).

Real-time analyses of live cells expressing EGFP-tagged patch assembly proteins revealed that different proteins are recruited in a sequential manner (Kaksonen *et al.*, 2003). For example, Las17p and Sla1p appeared at patches at early time points and were later joined by Abp1p and actin filaments. Therefore, in wild-type cells that undergo constitutive turnover of actin patches, Las17p patches partially colocalize with Abp1p patches. In contrast, in the *sla2*Δ mutant, in which actin patches are immobilized, Las17p patches basically colocalize with Abp1p patches. In the *cdc50*Δ *erg3*Δ mutant, 54% of cytoplasmic Las17p-EGFP patches were colocalized with Abp1p tagged with mRFP1 (n = 230 patches; Figure 5C).

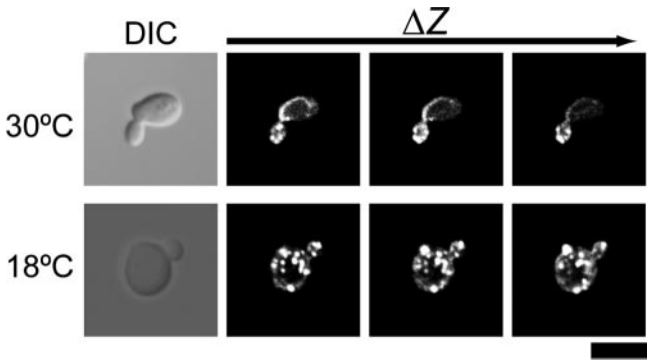

Figure 10. Confocal microscopic observations of cytoplasmic actin patches in the *rcy1*Δ mutant. KKT133 (*rcy1*Δ) was cultured in YP-DAW at 18°C or 30°C for 9 h, followed by staining with TRITC-phalloidin as described in Figure 3A. Three consecutive *z*-focal planes are shown. Bar, 5 μm.

Conversely, 74% of cytoplasmic Abp1p-mRFP1 patches were colocalized with Las17p-EGFP (n = 168 patches). Similarly, 67% of cytoplasmic Myo5p-EGFP patches colocalized with Abp1p-mRFP1 (n = 170 patches), and 64% of cytoplasmic Abp1p-mRFP1 patches colocalized with Myo5p-EGFP (n = 191 patches). The ratios of colocalization of these proteins were very similar in patches at cortical sites both in *cdc50*Δ *erg3*Δ mutant and wild-type cells (our unpublished data). Our results suggest that the mechanisms of assembly and turnover of the cytoplasmic actin patches seen in the *cdc50*Δ *erg3*Δ mutant are similar to those that govern assembly and turnover of normal cortical actin patches.

Intracellular Formation of Actin Patches May Be Dependent on Endocytosis

To further investigate the process of intracellular actin patch assembly in the *cdc50*Δ *erg3*Δ mutant, we constructed *cdc50*Δ *erg3*Δ mutants harboring additional mutations in genes that regulate the establishment of cell polarity (*cdc42-1*), actin cable assembly (*bni1-116 bnr1*Δ), or cortical actin patch assembly (*arp2-1* and *las17-11*). Neither *cdc42-1* nor *bni1-116 bnr1*Δ mutation affected the cytoplasmic localization of actin patches in the *cdc50*Δ *erg3*Δ mutant (Figure 6A). In contrast, both the *arp2-1* and *las17-11* mutations inhibited the cytoplasmic assembly of actin patches (Figure 6A). These results suggest that the actin patch machinery is involved in the assembly of intracellular patches. However, inhibition of endocytosis may be a prerequisite for this observed disappearance of cytoplasmic actin patches. Because it was not possible to discriminate between these possibilities by using actin patch machinery mutants, we opted to cells with the actin inhibitor LAT-A to inhibit endocytosis. LAT-A treatment inhibits endocytic internalization by interfering with actin polymerization. As described above, because recruitment of actin patch components precedes the assembly of actin and Abp1p, Las17p-EGFP patches can be assembled at cortical sites in the presence of LAT-A (Kaksonen *et al.*, 2003). Thus, we incubated a *cdc50*Δ *erg3*Δ mutant expressing Abp1p-mRFP1 and Las17p-EGFP for 1 h in the presence of LAT-A after 8 h depletion of Cdc50p. This treatment led to diffuse cytoplasmic staining of Abp1p-mRFP1 (Figure 6B). In contrast, LAT-A treatment did not affect patch assembly of Las17p-EGFP at cortical sites, but did inhibit patch assembly within the cytoplasm (Figure 6B). These results suggest that endocytosis is required for cytoplasmic formation of Las17p-EGFP patches, and thus for assembly of intracellular actin patches.

*The cdc50*Δ *erg3*Δ *Mutant Is Defective in Endocytic Recycling of Snc1p and Sterols*

The endocytosis-dependent assembly of cytoplasmic actin patches in the *cdc50*Δ *erg3*Δ mutant suggests that these actin patches are assembled on internal membranes derived from the endocytic processes. To further examine endocytosis in the *cdc50*Δ *erg3*Δ mutant, cells were incubated with FM4-64 at 30°C. Both *cdc50*Δ and *erg3*Δ single mutants, as well as wild-type cells, internalized FM4-64 and delivered it to the vacuole after 60-min chase (Figure 7A). Similarly, the *cdc50*Δ *erg3*Δ mutant also internalized and transported FM4-64 to the vacuole. These results suggest that the *cdc50*Δ *erg3*Δ mutant is not defective in either endocytic internalization or transport to the vacuole. However, the FM4-64 labeling revealed vacuole fragmentation in the *cdc50*Δ *erg3*Δ mutant. Interestingly, ergosterol has been implicated in vacuole fusion (Fratti *et al.*, 2004), and it is possible that phospholipid asymmetry may also play a role.

We next examined endocytic recycling in the *cdc50*Δ *erg3*Δ mutant. The exocytic v-SNARE Snc1p follows a recycling route from the plasma membrane via early endosomes to the TGN (Lewis *et al.*, 2000). In the *erg3*Δ mutant, green fluorescent protein (GFP)-tagged Snc1p was localized mainly to polarized plasma membrane sites in a manner similar to that of wild-type cells. In P_{GAL1}-*3HA-CDC50* cells depleted of Cdc50p for 9 h, GFP-Snc1p was only faintly visible at the plasma membrane, and 20% of the cells contained internal punctate structures of GFP-Snc1p (n = 158; Figure 7A). This phenotype is not as severe as that of the *cdc50* null mutant (Saito *et al.*, 2004), suggesting that the 9-h incubation does not completely deplete Cdc50p. In contrast, the *cdc50*Δ *erg3*Δ mutant exhibited much more severe defects after 9-h depletion of Cdc50p (Figure 7A). In 69% of *cdc50*Δ *erg3*Δ mutant cells, GFP-Snc1p was localized only in internal structures (n = 118). These GFP-Snc1p-containing structures were distinct from vacuoles stained with FM4-64 (Figure 7B). To address whether these punctate GFP-Snc1p structures were formed via the endocytic pathway, we examined GFP-Snc1p localization in the presence or absence of LAT-A, which blocks the internalization of Snc1p. In the presence of LAT-A, GFP-Snc1p was localized at the plasma membrane, although a fraction was still diffusely localized in the cytoplasm (Figure 7C). Taken together, these results suggest that the *cdc50*Δ *erg3*Δ mutant exhibits defective endocytic recycling. Consistently, the *erg3*Δ mutation exhibited synthetic lethality with mutations that impair endocytic recycling, but not with mutations that impair other pathways of vesicle traffic (Table 3).

The above results raised the possibility that the observed intracellular actin patches are assembled on membranes accumulated in the absence of efficient endocytic recycling. We thus examined the localization of Abp1p-EGFP and mRFP1-Snc1p when coexpressed in the *cdc50*Δ *erg3*Δ mutant. If cytoplasmic actin patches are assembled on Snc1p-containing membranes, they should be found inside of (completely overlapping) or in contact with (partially overlapping) the mRFP1-Snc1p-containing area. Because endocytic internalization normally occurs in the *cdc50*Δ *erg3*Δ mutant, cortical actin patches that function in this pathway should be also present in the *cdc50*Δ *erg3*Δ mutant. In addition, Abp1p-EGFP patches move a relatively long distance (500–1000 nm) toward the cell center from the cortex (Kaksonen *et al.*, 2003). To distinguish these Abp1p-EGFP patches, the cell periphery and a position 500 nm distant from the plasma mem-

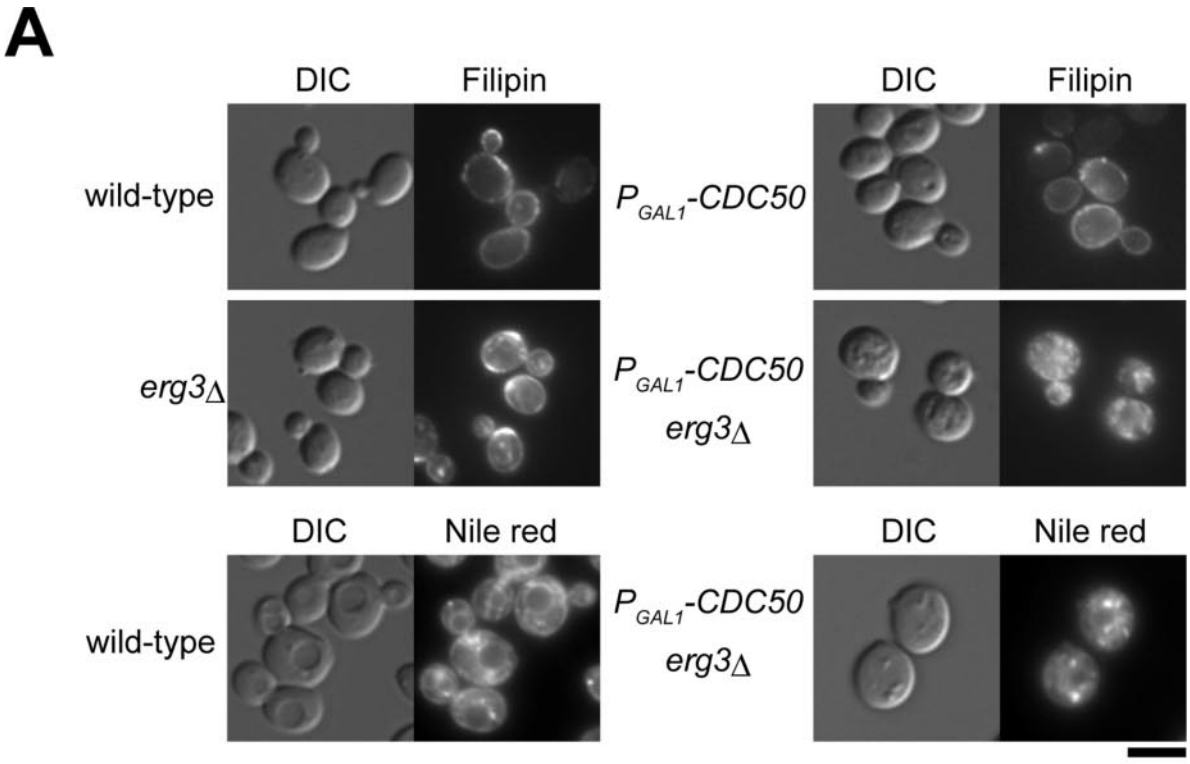
A
DIC
Filipin
wild-type
P_{GAL1}-CDC50
erg3Δ
P_{GAL1}-CDC50 erg3Δ
DIC
Nile red
wild-type
P_{GAL1}-CDC50 erg3Δ

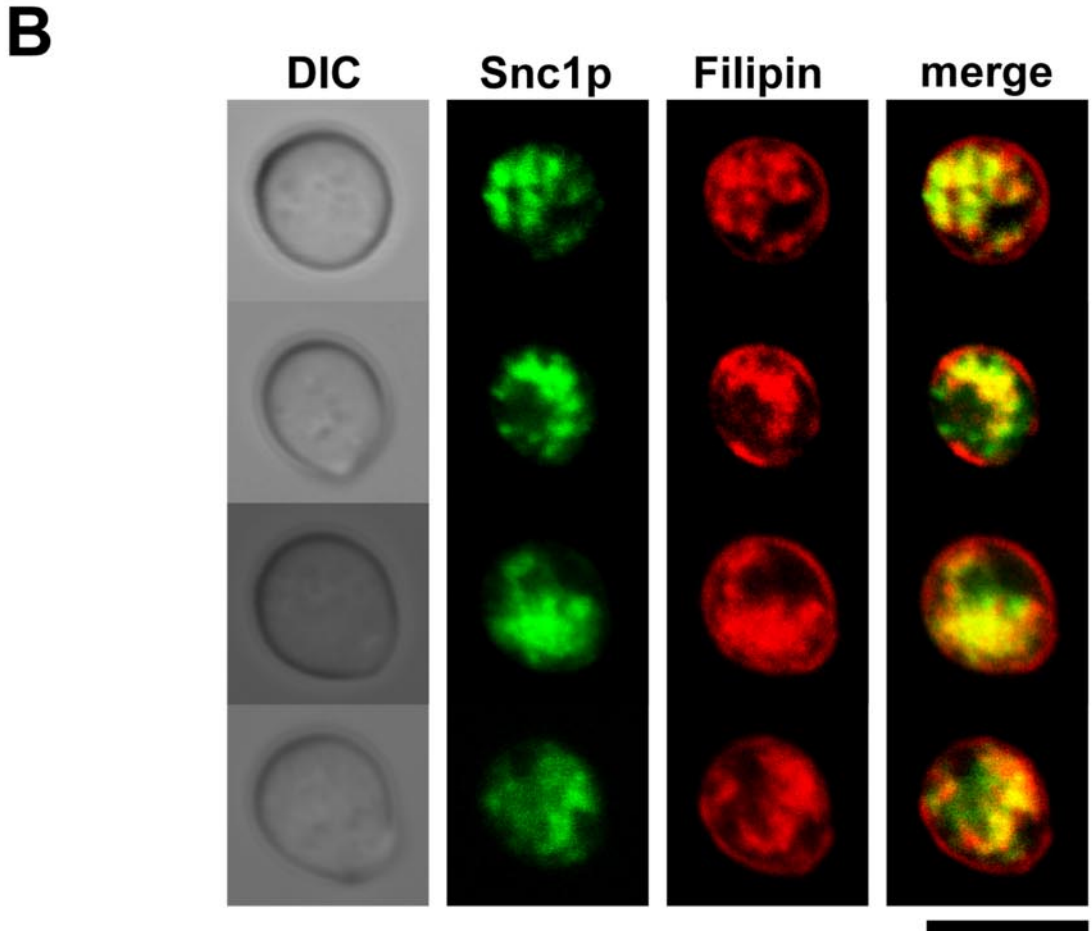
B
DIC
Snc1p
Filipin
merge

Figure 11.

brane are indicated with solid and broken lines, respectively, in images of confocal microscopy (Figure 8A). Eighty percent of cytoplasmic Abp1p-EGFP-patches (n = 218) showed completely (40.8%) or partially (39.4%) overlapping localization with the mRFP1-Snc1p-containing membranes (Figure 8, A and B). We further examined the localization of cytoplasmic Abp1p-EGFP patches that did not show colocalization with Snc1p membranes in one focal plane. When 30 individual patches were examined along the *z*-axis by confocal microscopy, all these patches overlapped mRFP1-Snc1p signals. Representative images of these patches are shown in Figure 8C. These results suggest that the intracellular actin patches are indeed formed on the surface of unrecycled endocytosed membranes.

Next, we examined the *cdc50*Δ *erg3*Δ mutant cells at the ultrastructural level. The *drs2*Δ mutant accumulates large and abnormal double-membrane structures with crescent- or ring-shaped morphology (Chen *et al.*, 1999; Hua *et al.*, 2002). These structures were observed in the *cdc50*Δ mutant, but not in either *erg3*Δ mutant or wild-type cells. In contrast, these structures were massively accumulated in the *cdc50*Δ *erg3*Δ mutant (Figure 9). These abnormal structures may represent the Snc1p-containing structures shown in Figure 8A. A mutant in *RCY1* encoding an F-box protein also accumulates large membranous structures due to defective endocytic recycling as assessed by electron microscopy (Wiederkehr *et al.*, 2000). Interestingly, intracellular actin patches were also assembled in 32% (n = 275) of *rcy1*Δ mutant cells at a nonpermissive temperature for growth, 18°C (Figure 10). In contrast, the *ypt6*Δ mutant, which accumulates recycling endocytic vesicles rather than large membranous structures (Siniossoglou *et al.*, 2000), did not exhibit intracellular assembly of actin patches (our unpublished data). Thus, *cdc50*Δ *erg3*Δ and *rcy1*Δ mutants seem to accumulate similar endocytosed membranes that serve as a site for assembly of actin patches.

The observation that *erg3* mutation exacerbated the defect in endocytic recycling of Snc1p exhibited by the *cdc50*Δ mutant prompted us to examine the cellular distribution of sterols. Staining of wild-type cells with filipin, a fluorescent indicator for sterols which is effective in both yeast and mammalian cells (Beh and Rine, 2004), revealed that ergosterol is most abundant in the plasma membrane (Figure 11A). Essentially the same results were obtained for both *erg3*Δ and *cdc50*Δ cells, suggesting that the ergosterol-related molecules stained with filipin are also enriched in the plasma membranes of these cells. However, in the *cdc50*Δ *erg3*Δ mutant, filipin/sterol fluorescence was predominantly detected either diffusely within the cytosol or as punctate dots, with a concomitant decrease in plasma membrane staining (Figure 11A, top panels). The intracellular staining of sterols may reflect the accumulation of sterols in lipid particles, which are lipid storage compartments stainable with the fluorescence dye Nile red (Verstrepen *et al.*, 2004). However, as shown in the bottom panels of Figure 11A, neither the number nor the size of lipid particles was significantly different between wild-type and *cdc50*Δ *erg3*Δ mutant cells. These results suggest that the *cdc50*Δ *erg3*Δ mutant is defective in the sorting of sterols to the plasma membrane. Interestingly, the *cdc50*Δ single mutant exhibited plasma membrane sterol distribution similar to wild-type cells under conditions that cause Snc1p to be accumulated in the cytoplasmic space in these cells (12-h depletion of Cdc50p; Figure 11A, top panel). This sterol distribution phenotype is thus similar to that observed for the actin cytoskeleton in the *cdc50*Δ single mutant, characterized by normally organized actin cables and cortical actin patches.

The cytoplasmic accumulation of both sterols and GFP-Snc1p in the *cdc50*Δ *erg3*Δ mutant raises the possibility that sterols accumulate in Snc1p-containing membranes. We performed filipin staining in *cdc50*Δ *erg3*Δ cells expressing GFP-Snc1p and compared their signals. As shown in Figure 11B, filipin-positive structures overlapped GFP-Snc1p, suggesting that Snc1p-containing membranes are rich in sterols. Together with the results that Abp1p-EGFP patches were assembled on the mRFP1-Snc1p-containing membranes (Figure 8), our results also suggest that actin patches are assembled on sterol-rich endocytic membranes in the *cdc50*Δ *erg3*Δ mutant. Interestingly, some GFP-positive structures did not exhibit filipin signals and vice versa (see merged images), possibly reflecting compartmentalized structures of the accumulated endosomal membranes.

Figure 11 (facing page). Sterol distribution in Cdc50p-depleted *erg3*Δ mutant cells. (A) Strains described in Figure 2A were cultured in YPDAW at 30°C for 12 h. Cells were fixed, and sterols were stained with filipin, followed by a microscopic observation visualized by DIC and epifluorescence (top panels). Lipid particles were similarly detected by staining with Nile red (bottom panels). (B) Colocalization of sterols with Snc1p-containing membranes in the *cdc50*Δ *erg3*Δ mutant. The strain KKT16 (P_{GAL1}-*3HA-CDC50 erg3*Δ) containing pRS416-GFP-SNC1 was cultured in SDAW-Ura at 30°C for 12 h, and the cells were stained with filipin, followed by a confocal microscopic observation. Images are central focal planes. Bars, 5 μm.

DISCUSSION

Requirement of a Putative Phospholipid Translocase and Ergosterol in Endocytic Vesicular Transport

Some *erg*Δ mutants exhibit reduced endocytic internalization and transport to the vacuole after internalization (Munn *et al.*, 1999; Heese-Peck *et al.*, 2002). We did not observe a defect in endocytic internalization in the *cdc50*Δ *erg3*Δ mutant, as assayed by FM4-64 uptake. The efficiency of endocytic transport from the plasma membrane to the vacuole was difficult to measure in the *cdc50*Δ *erg3*Δ mutant as a result of vacuole fragmentation. In contrast, the *cdc50*Δ *erg3*Δ mutant did exhibit defects in endocytic recycling. The *cdc50*Δ mutant intracellularly accumulates Snc1p-containing membranous structures (Saito *et al.*, 2004) and *erg3*Δ mutation dramatically exacerbated this defect. The involvement of ergosterol in endocytic recycling is supported by the synthetic lethal interactions of *erg3*Δ mutation with mutations that impair endocytic recycling.

One important function of endocytic recycling is to retrieve lipids that are most abundant in the plasma membrane, such as sterols and sphingolipid. Accumulation of sterol-containing membranes in the *cdc50*Δ *erg3*Δ mutant was revealed by filipin staining, suggesting that this mutant cannot recycle sterols to the plasma membrane, most likely secondary to a defect in endocytic recycling. Interestingly, filipin-stained membranes did not accumulate in the *cdc50*Δ single mutant, in clear contrast to the accumulation of Snc1p-containing structures in this mutant. It is possible that there exists an alternate, nonvesicular route for retrieval of ergosterol from endocytic compartments to the plasma membrane, in addition to the endocytic recycling pathway (e.g., sterol transfer protein; Soccio and Breslow, 2004). Thus, the nonergosterol sterols accumulated in the *erg3*Δ mutant may be recycled to the plasma membrane by the endocytic recycling pathway, but not by this alternative pathway,

possibly accounting for the observation of intracellular sterol accumulation only in the *cdc50*Δ *erg3*Δ double mutant.

Electron microscopy revealed that large membranous structures, rather than vesicle-like structures, are the main components of the accumulated matter in the *cdc50*Δ *erg3*Δ mutant. Together with the defects in endocytic recycling, these accumulated membranes may be derived from endocytic recycling compartments. One proposed role for phospholipid asymmetry is to drive the formation of vesicles by recruiting machinery for vesicle budding or by inducing physical deformation of the membrane (Pomorski *et al.,* 2004). The lack of mature ergosterol may exacerbate the vesicle budding defects resulting from possible loss of phospholipid asymmetry in the *cdc50*Δ mutant.

*Possible Effects of the cdc50*Δ *and erg3*Δ *Mutations on the Physical Properties of Endosomal Membrane Bilayers*

Given that the endosomal Cdc50p-Drs2p complex is involved in endocytic recycling of Snc1p, the recycling of ergosterol through the endocytic pathway suggests that possible loss of phospholipid asymmetry and the lack of mature ergosterol affect the same lipid bilayers of early endosomes or TGN in the *cdc50*Δ *erg3*Δ mutant. We previously suggested that Cdc50p-Drs2p can translocate phosphatidylethanolamine and PS to the cytoplasmic face of bilayers when Cdc50p-Drs2p is forced to localize to the plasma membrane (Saito *et al.,* 2004). In vitro studies using isolated Golgi membranes also suggested that Drs2p translocates PS (Natarajan *et al.,* 2004). It has thus been suggested that the endosomal/TGN membranes of the *cdc50*Δ mutant have less aminophospholipids in their cytoplasmic leaflets. In contrast to phospholipids, cholesterol is believed to translocate across the membrane without the requirement for energy input (Hamilton, 2003), suggesting that the nonergosterol sterols are distributed in both bilayer leaflets in the *erg3*Δ mutant. Biophysical studies suggest that the head groups of phospholipids can affect the behavior of cholesterol in chemically defined lipid bilayers. At high concentrations within the membrane, cholesterol readily forms aggregates or crystallites, presumably as a consequence of its relatively rigid fused ring structure. However, cholesterol aggregates are more readily formed in membranes containing PS than phosphatidylcholine, even when molar ratios and attached acyl chains are identical (Epand *et al.,* 2002). Irregular interactions between the phospholipid head groups and sterols present in the inner and/or outer surface(s) of the endosomal lipid bilayers might underlie the defective endocytic vesicle formation of the *cdc50*Δ *erg3*Δ mutant.

Roles for Sterols and a Putative Phospholipid Translocase in Polarized Actin Organization

Mislocalization of EGFP-Cdc42p in the *cdc50*Δ *erg3*Δ mutant may account for the mislocalization of its effectors, Bni1p-EGFP and Gic1p-EGFP, and thus for depolarized organization of actin cables resulting in nonpolarized cell growth. Polarized transport of Cdc42p is accomplished by Myo2p-driven vesicle transport (Wedlich-Soldner *et al.,* 2004). This is counteracted by endocytic internalization of Cdc42p from the plasma membrane (Irazoqui *et al.,* 2005). Locally exocytosed proteins will remain polarized if they are endocytosed and recycled before they can diffuse to equilibrium. Polarized localization of Snc1p was shown to be maintained by this mechanism (Valdez-Taubas and Pelham, 2003). Cdc42p may also remain polarized via recycling through the endocytic pathway, which is defective in the *cdc50*Δ *erg3*Δ mutant. Cdc42p has been implicated in polarized assembly of cortical actin patches (Lechler *et al.,* 2001). However, the intracellular assembly of actin patches observed here occurred independently of Cdc42p, suggesting that Cdc42p is not directly involved in spatial control of actin patch assembly.

The Lipid Environment May Be a Determinant for Actin Patch Assembly Sites

One possible mechanism to explain the presence of cytoplasmic actin patches is that actin patches formed during endocytic internalization were not effectively disassembled even by the later phases of endocytic transport. Endocytic vesicles formed at the plasma membrane appear to carry polymerized actin and Abp1p for a significant duration, on the order of seconds, after internalization (Kaksonen *et al.,* 2003; Huckaba *et al.,* 2004). In mutants that exhibit inhibition of actin patch disassembly, such as *sla2* and *ark1 prk1*, endocytic internalization is inhibited because of formation of immobilized actin clumps consisting of actin and patch assembly proteins (Kaksonen *et al.,* 2003; Sekiya-Kawasaki *et al.,* 2003). However, the *cdc50*Δ *erg3*Δ mutant showed normal uptake of FM4-64 and did not show actin clump formation, suggesting that the assembled actin patches on the plasma membrane are successfully turned over to some significant extent.

The other more likely possibility is that the actin patches in this mutant are newly assembled on previously endocytosed internal membranes. In the case of endocytosis of Ste2p, it is thought that phosphorylation and ubiquitination of Ste2p is a prerequisite for the assembly of actin patch-associated proteins (Engqvist-Goldstein and Drubin, 2003). If actin patch assembly is generally initiated via a similar mechanism by a membrane-spanning cargo protein, this protein may be trapped in the endocytic membranes accumulated in the *cdc50*Δ *erg3*Δ mutant, resulting in intracellular assembly of actin patches. However, actin patches are normally disassembled after internalization of endocytic vesicles, suggesting that the ability of the membrane-spanning cargo protein to initiate actin assembly is normally suppressed on endosomal membranes. The endocytic membranes accumulated in the *cdc50*Δ *erg3*Δ mutant may be similar to the plasma membrane with respect to lipid composition (e.g., rich in sterols and sphingolipids) and thus may induce assembly of actin patches. However, defects in structural integrity of ergosterol and possible loss of phospholipid asymmetry do not seem to comprise a direct cause for actin patch assembly on endocytosed membranes, because the *rcy1*Δ mutant also assembled actin patches intracellularly. Interestingly, the *cdc50*Δ single mutant displays normal polarized organization of cortical actin patches and actin cables at 30°C, even while exhibiting the intracellular accumulation of Snc1p-containing membranous structures. Because the *cdc50*Δ single mutant does not accumulate sterols intracellularly, the assembly of actin patches on accumulated membranes may require the presence of sterols.

In conclusion, possible loss of phospholipid asymmetry and defects in sterol structural integrity lead to a defect in endocytic recycling, bringing about the accumulation of endocytic membranes onto which actin patches are assembled. In addition, the *cdc50*Δ *erg3*Δ mutant, which demonstrates ectopic assembly of actin patches on internal membranes, represents a powerful system that can be exploited to enable a search for factors (proteins or/and lipids) in vitro that are required for actin patch assembly.

ACKNOWLEDGMENTS

We specially thank Hideyuki Matsuura for GC-MS of sterols. We would also like to thank David Drubin, Howard Riezman, Charles Boone, Yoshimi Takai, Akihiko Nakano, and Barbara Winsor for yeast strains and plasmids; Ramon Serrano for the anti-Pma1p-antibody; Taisuke Miyazaki, Takashi Ueda, and Aiko Hirata for electron microscopic instructions; and Eriko Itoh for her technical assistance. We thank Konomi Kamada and members of the Tanaka lab for valuable suggestions on the course of these experiments. This work was supported by grants-in-aid for Scientific Research from the Ministry of Education, Culture, Sports, Science, and Technology, Japan, to T.Y. and K.T.

REFERENCES

Ayscough, K. R., Stryker, J., Pokala, N., Sanders, M., Crews, P., and Drubin, D. G. (1997). High rates of actin filament turnover in budding yeast and roles for actin in establishment and maintenance of cell polarity revealed using the actin inhibitor latrunculin-A. J. Cell Biol. *137*, 399–416.

Bagnat, M., Keranen, S., Shevchenko, A., Shevchenko, A., and Simons, K. (2000). Lipid rafts function in biosynthetic delivery of proteins to the cell surface in yeast. Proc. Natl. Acad. Sci. USA *97*, 3254–3259.

Bagnat, M., and Simons, K. (2002). Cell surface polarization during yeast mating. Proc. Natl. Acad. Sci. USA *99*, 14183–14188.

Beh, C. T., and Rine, J. (2004). A role for yeast oxysterol-binding protein homologs in endocytosis and in the maintenance of intracellular sterol-lipid distribution. J. Cell Sci. *117*, 2983–2996.

Bensen, E. S., Costaguta, G., and Payne, G. S. (2000). Synthetic genetic interactions with temperature-sensitive clathrin in *Saccharomyces cerevisiae*: roles for synaptojanin-like Inp53p and dynamin-related Vps1p in clathrin-dependent protein sorting at the trans-Golgi network. Genetics *154*, 83–97.

Brachmann, C. B., Davies, A., Cost, G. J., Caputo, E., Li, J., Hieter, P., and Boeke, J. D. (1998). Designer deletion strains derived from *Saccharomyces cerevisiae* S288C: a useful set of strains and plasmids for PCR-mediated gene disruption and other applications. Yeast *14*, 115–132.

Chen, C. Y., Ingram, M. F., Rosal, P. H., and Graham, T. R. (1999). Role for Drs2p, a P-type ATPase and potential aminophospholipid translocase, in yeast late Golgi function. J. Cell Biol. *147*, 1223–1236.

Drubin, D. G., and Nelson, W. J. (1996). Origins of cell polarity. Cell *84*, 335–344.

Elble, R. (1992). A simple and efficient procedure for transformation of yeasts. Biotechniques *13*, 18–20.

Engqvist-Goldstein, A. E., and Drubin, D. G. (2003). Actin assembly and endocytosis: from yeast to mammals. Annu. Rev. Cell Dev. Biol. *19*, 287–332.

Epand, R. M., Bain, A. D., Sayer, B. G., Bach, D., and Wachtel, E. (2002). Properties of mixtures of cholesterol with phosphatidylcholine or with phosphatidylserine studied by ^{13}C magic angle spinning nuclear magnetic resonance. Biophys. J. *83*, 2053–2063.

Evangelista, M., Zigmond, S., and Boone, C. (2003). Formins: signaling effectors for assembly and polarization of actin filaments. J. Cell Sci. *116*, 2603–2611.

Fratti, R. A., Jun, Y., Merz, A. J., Margolis, N., and Wickner, W. (2004). Interdependent assembly of specific regulatory lipids and membrane fusion proteins into the vertex ring domain of docked vacuoles. J. Cell Biol. *167*, 1087–1098.

Geli, M. I., and Riezman, H. (1996). Role of type I myosins in receptor-mediated endocytosis in yeast. Science *272*, 533–535.

Gietz, R. D., and Sugino, A. (1988). New yeast-*Escherichia coli* shuttle vectors constructed with *in vitro* mutagenized yeast genes lacking six-base pair restriction sites. Gene *74*, 527–534.

Gietz, R. D., and Woods, R. A. (2002). Transformation of yeast by lithium/acetate/single-stranded carrier DNA/polyethylene glycol method. Methods Enzymol. *350*, 87–96.

Goldstein, A. L., Pan, X., and McCusker, J. H. (1999). Heterologous *URA3MX* cassettes for gene replacement in *Saccharomyces cerevisiae*. Yeast *15*, 507–511.

Gurunathan, S., David, D., and Gerst, J. E. (2002). Dynamin and clathrin are required for the biogenesis of a distinct class of secretory vesicles in yeast. EMBO J. *21*, 602–614.

Gueldener, U., Heinisch, J., Koehler, G. J., Voss, D., and Hegemann, J. H. (2002). A second set of *loxP* marker cassettes for Cre-mediated multiple gene knockouts in budding yeast. Nucleic Acids Res. *30*, e23.

Guthrie, C., and Fink, G. R., eds. (1991). Guide to yeast genetics and molecular biology. Methods Enzymology, Vol. 194, San Diego: Academic Press.

Hamilton, J. A. (2003). Fast flip-flop of cholesterol and fatty acids in membranes: implications for membrane transport proteins. Curr. Opin. Lipidol. *14*, 263–271.

Heese-Peck, A., Pichler, H., Zanolari, B., Watanabe, R., Daum, G., and Riezman, H. (2002). Multiple functions of sterols in yeast endocytosis. Mol. Biol. Cell *13*, 2664–2680.

Hua, Z., Fatheddin, P., and Graham, T. R. (2002). An essential subfamily of Drs2p-related P-Type ATPases is required for protein trafficking between Golgi complex and endosomal/vacuolar system. Mol. Biol. Cell *13*, 3162–3177.

Huckaba, T. M., Gay, A. C., Pantalena, L. F., Yang, H. C., and Pon, L. A. (2004). Live cell imaging of the assembly, disassembly, and actin cable-dependent movement of endosomes and actin patches in the budding yeast, *Saccharomyces cerevisiae*. J. Cell Biol. *167*, 519–530.

Irazoqui, J. E., Howell, A. S., Theesfeld, C. L., and Lew, D. J. (2005). Opposing roles for actin in Cdc42p polarization. Mol. Biol. Cell *16*, 1296–1304.

Janmey, P. A., and Lindberg, U. (2004). Cytoskeletal regulation: rich in lipids. Nat. Rev. Mol. Cell. Biol. *5*, 658–666.

Johnson, D. I., and Pringle, J. R. (1990). Molecular characterization of *CDC42*, a *Saccharomyces cerevisiae* gene involved in the development of cell polarity. J. Cell Biol. *111*, 143–152.

Kaiser, C. A., and Schekman, R. (1990). Distinct sets of *SEC* genes govern transport vesicle formation and fusion early in the secretory pathway. Cell *61*, 723–733.

Kadota, J., Yamamoto, T., Yoshiuchi, S., Bi, E., and Tanaka, K. (2004). Septin ring assembly requires concerted action of polarisome components, a PAK kinase Cla4p, and the actin cytoskeleton in *Saccharomyces cerevisiae*. Mol. Biol. Cell *15*, 5329–5345.

Kaksonen, M., Sun, Y., and Drubin, D. G. (2003). A pathway for association of receptors, adaptors, and actin during endocytic internalization. Cell *115*, 475–487.

Koshland, D., Kent, J. C., and Hartwell, L. H. (1985). Genetic analysis of the mitotic transmission of minichromosomes. Cell *40*, 393–403.

Lechler, T., Jonsdottir, G. A., Klee, S. K., Pellman, D., and Li, R. (2001). A two-tiered mechanism by which Cdc42 controls the localization and activation of an Arp2/3-activating motor complex in yeast. J. Cell Biol. *155*, 261–270.

Lewis, M. J., Nichols, B. J., Prescianotto-Baschong, C., Riezman, H., and Pelham, H. R. (2000). Specific retrieval of the exocytic SNARE Snc1p from early yeast endosomes. Mol. Biol. Cell *11*, 23–38.

Longtine, M. S., McKenzie, A., 3rd, Demarini, D. J., Shah, N. G., Wach, A., Brachat, A., Philippsen, P., and Pringle, J. R. (1998). Additional modules for versatile and economical PCR-based gene deletion and modification in *Saccharomyces cerevisiae*. Yeast *14*, 953–961.

Lucero, H. A., and Robbins, P. W. (2004). Lipid rafts-protein association and the regulation of protein activity. Arch. Biochem. Biophys. *426*, 208–224.

Martin, S. W., and Konopka, J. B. (2004). Lipid raft polarization contributes to hyphal growth in *Candida albicans*. Eukaryot. Cell *3*, 675–684.

Madania, A., Dumoulin, P., Grava, S., Kitamoto, H., Scharer-Brodbeck, C., Soulard, A., Moreau, V., and Winsor, B. (1999). The *Saccharomyces cerevisiae* homologue of human Wiskott-Aldrich syndrome protein Las17p interacts with the Arp2/3 complex. Mol. Biol. Cell *10*, 3521–3538.

Misu, K., Fujimura-Kamada, K., Ueda, T., Nakano, A., Katoh, H., and Tanaka, K. (2003). Cdc50p, a conserved endosomal membrane protein, controls polarized growth in *Saccharomyces cerevisiae*. Mol. Biol. Cell *14*, 730–747.

Mochida, J., Yamamoto, T., Fujimura-Kamada, K., and Tanaka, K. (2002). The novel adaptor protein, Mti1p, and Vrp1p, a homolog of Wiskott-Aldrich syndrome protein-interacting protein (WIP), may antagonistically regulate type I myosins in *Saccharomyces cerevisiae*. Genetics *160*, 923–934.

Munn, A. L., Heese-Peck, A., Stevenson, B. J., Pichler, H., and Riezman, H. (1999). Specific sterols required for the internalization step of endocytosis in yeast. Mol. Biol. Cell *10*, 3943–3957.

Natarajan, P., Wang, J., Hua, Z., and Graham, T. R. (2004). Drs2p-coupled aminophospholipid translocase activity in yeast Golgi membranes and relationship to *in vivo* function. Proc. Natl. Acad. Sci. USA *101*, 10614–10619.

Pomorski, T., Holthuis, J. C., Herrmann, A., and van Meer, G. (2004). Tracking down lipid flippases and their biological functions. J. Cell Sci. *117*, 805–813.

Prinz, W. (2002). Cholesterol trafficking in the secretory and endocytic systems. Semin. Cell Dev. Biol. *13*, 197–203.

Pruyne, D., and Bretscher, A. (2000a). Polarization of cell growth in yeast. II. The role of the cortical actin cytoskeleton. J. Cell Sci. *113*, 571–585.

Pruyne, D., and Bretscher, A. (2000b). Polarization of cell growth in yeast. I. Establishment and maintenance of polarity states. J. Cell Sci. *113*, 365–375.

Pruyne, D. W., Schott, D. H., and Bretscher, A. (1998). Tropomyosin-containing actin cables direct the Myo2p-dependent polarized delivery of secretory vesicles in budding yeast. J. Cell Biol. *143*, 1931–1945.

Rose, M. D., Winston, F., and Hieter, P. (1990). Methods in Yeast Genetics: A Laboratory Course Manual, Cold Spring Harbor, NY: Cold Spring Harbor Laboratory Press.

Saito, K., Fujimura-Kamada, K., Furuta, N., Kato, U., Umeda, M., and Tanaka, K. (2004). Cdc50p, a protein required for polarized growth, associates with the Drs2p P-type ATPase implicated in phospholipid translocation in *Saccharomyces cerevisiae*. Mol. Biol. Cell *15*, 3418–3432.

Seeley, E. S., Kato, M., Margolis, N., Wickner, W., and Eitzen, G. (2002). Genomic analysis of homotypic vacuole fusion. Mol. Biol. Cell *13*, 782–794.

Sekiya-Kawasaki, M. *et al*. (2003). Dynamic phosphoregulation of the cortical actin cytoskeleton and endocytic machinery revealed by real-time chemical genetic analysis. J. Cell Biol. *162*, 765–772.

Sikorski, R. S., and Hieter, P. (1989). A system of shuttle vectors and yeast host strains designed for efficient manipulation of DNA in *Saccharomyces cerevisiae*. Genetics *122*, 19–27.

Siniossoglou, S., Peak-Chew, S. Y., and Pelham, H. R. (2000). Ric1p and Rgp1p form a complex that catalyses nucleotide exchange on Ypt6p. EMBO J. *19*, 4885–4894.

Soccio, R. E., and Breslow, J. L. (2004). Intracellular cholesterol transport. Arterioscler. Thromb. Vasc. Biol. *24*, 1150–1160.

Toi, H., Fujimura-Kamada, K., Irie, K., Takai, Y., Todo, S., and Tanaka, K. (2003). She4p/Dim1p interacts with the motor domain of unconventional myosins in the budding yeast, *Saccharomyces cerevisiae*. Mol. Biol. Cell *14*, 2237–2249.

Valdez-Taubas, J., and Pelham, H. R. (2003). Slow diffusion of proteins in the yeast plasma membrane allows polarity to be maintained by endocytic cycling. Curr. Biol. *13*, 1636–1640.

Verstrepen, K. J., Van Laere, S. D., Vercammen, J., Derdelinckx, G., Dufour, J. P., Pretorius, I. S., Winderickx, J., Thevelein, J. M., and Delvaux, F. R. (2004). The *Saccharomyces cerevisiae* alcohol acetyl transferase Atf1p is localized in lipid particles. Yeast *21*, 367–377.

Wedlich-Soldner, R., Wai, S. C., Schmidt, T., and Li, R. (2004). Robust cell polarity is a dynamic state established by coupling transport and GTPase signaling. J. Cell Biol. *166*, 889–900.

Wesp, A., Hicke, L., Palecek, J., Lombardi, R., Aust, T., Munn, A. L., and Riezman, H. (1997). End4p/Sla2p interacts with actin-associated proteins for endocytosis in *Saccharomyces cerevisiae*. Mol. Biol. Cell *8*, 2291–2306.

Wiederkehr, A., Avaro, S., Prescianotto-Baschong, C., Haguenauer-Tsapis, R., and Riezman, H. (2000). The F-box protein Rcy1p is involved in endocytic membrane traffic and recycling out of an early endosome in *Saccharomyces cerevisiae*. J. Cell Biol. *149*, 397–410.